EUROPEAN JOURNAL OF PURE AND APPLIED MATHEMATICS
2025, Vol. 18, Issue 2, Article Number 5851
ISSN 1307-5543 – ejpam.com
Published by New York Business Global

Harvesting Mixed, Homoclinic Breather, M-Shaped and Other Wave Profiles of the Heisenberg Ferromagnet-Type Akbota Equation

Baboucarr Ceesay[1,2], Muhammad Z. Baber[3], Nauman Ahmed[1,4], Muhammad Jawaz[1], Jorge E. Macías-Díaz[5,6,*], Armando Gallegos[7]

[1] *Mathematics and Statistics Department , The University of Lahore, Lahore, Pakistan*
[2] *Mathematics Unit, The University of The Gambia, The Gambia*
[3] *Department of Mathematics and Statistics, The University of Lahore Sargodha Campus, Sargodha, Pakistan*
[4] *Department of Computer Science and Mathematics, Lebanese American University, Beirut, Lebanon*
[5] *Department of Mathematics and Didactics of Mathematics, Tallinn University, Narva Rd. 25, 10120 Tallinn, Estonia*
[6] *Departamento de Matemáticas y Física, Universidad Autónoma de Aguascalientes, Aguascalientes 20131, México*
[7] *Departamento de Ciencias Exactas y Tecnología, Centro Universitario de los Lagos, Universidad de Guadalajara, Jalisco, Mexico*

Abstract. We use the Hirota bilinear technique to investigate wave solutions to the Heisenberg ferromagnetic-type Akbota problem arising in surface geometry. The equation is a crucial paradigm for examining and visualizing surface geometry and curve analysis. The equation is an integrable coupled model with soliton solutions. It is a key instrument for investigating nonlinear phenomena in differential geometry of curves and surfaces, magnetism, and optics. The solutions we explore are periodic lump waves, periodic cross-kink waves, homoclinic breather waves, M-shaped waves interacting with kink and rogue waves, and mixed waves. We derive exact solutions and carefully choose parameter values to generate a variety of three-dimensional graphs and the associated contour and density plots. The soliton phenomenon is explained by the physical structures and solutions discovered, which also replicate the dynamic characteristics of the traveling-wave deformation front that is created in the dispersive medium. It demonstrates the power, suitability, and potential applications of the Hirota bilinear technique in future research to identify unique solutions for a wide range of nonlinear model types found in engineering and physical science. These solutions are relevant in nonlinear fiber optics, magnetism and differential geometry.

2020 Mathematics Subject Classifications: 35C05

Key Words and Phrases: Heisenberg ferromagnet-type Akbota equation, Hirota bilinear transformation, periodic cross kink solution, lump solution, homoclinic M-shaped breather

1. Introduction

In recent years, there has been a significant focus on nonlinear partial differential Equations (NLPDEs) and their applications in several fields, including acoustic waves, nonlinear dynamics, condensed matter physics, optical fibers, chemical reactions, plasma dynamics, plasma physics,

*Corresponding author.
DOI: https://doi.org/10.29020/nybg.ejpam.v18i2.5851

Email addresses: bceesay@utg.edu.gm (B. Ceesay), zafarullah8883@gmail.com (M. Z. Baber), nauman.ahmed@math.uol.edu.pk (N. Ahmed), muhammad.jawaz@math.uol.edu.pk (M. Jawaz), jorge.maciasdiaz@edu.uaa.mx (J. E. Macías-Díaz), gallegos@culagos.udg.mx (A. Gallegos)

biological membrane, electromagnetic waves, etc. This has been the subject of both theoretical and experimental investigations. A lot of work has been done on nonlinear equations involving these fields lately in an effort to better understand their qualitative and quantitative characteristics. The ideal balancing act between dispersion effects and nonlinearity that produces a soliton pulse is a key characteristic of most nonlinear equations. Owing to its wealth of physical structures and scientific features, the study of integrable qualities for nonlinear evolution equations has become a research hot-point. Deriving nonlinear integrable equations that explain different physical events has garnered a lot of interest in recent decades, along with the integrability of nonlinear equations in general. In the field of nonlinear phenomena and solitary waves theory, discovering novel integrable systems has been a primary focus. Thus, from a theoretical as well as an experimental perspective, it is crucial to develop integrable NLPDEs that include higher-order elements. A significant amount of effort has been done by investigators in [1–8] to derive nonlinear integrable equations in $(n+1)$ dimensions, where $n = 1$, 2, and 3. In the domains of science and engineering, integrable equations which have a sizable number of conservation laws, Lax pairings, bi-Hamiltonian properties, and multiple soliton solutions are extensively studied [9–13]. Numerous research efforts have been dedicated to the derivation of novel integrable equations, utilizing potent techniques like recursion operators and the symmetries approach to accomplish this objective [14–18]. The integrability of the recently derived equations is verified using the Painlevé analysis [19–21].

The capacity of NLPDEs to describe nonlinear processes in the modern world lies in their ability to depict nonlinear events. Because of the advancements in computer technology, researchers have successfully solved a considerable number of these equations using mathematical and computational tools. Among those tools, the Hirota bilinear technique is a well-recognized and often employed approach to solving NLPDEs that have emerged in the past decades. If one knows the bilinear form, one may find the soliton solutions to the equation [22]. Several other potent techniques such as the Fan sub-equation and its modified form [23, 24], the Sardar-sub equation [25], the extended sinh-Gordon equation expansion [26], the $\frac{G'}{G^2}$-expansion [27], the Darboux transformation [28], the Lie group method [29], inverse scattering transformations [30], the generalized Jacobi elliptic function method [31] , the improved F-expansion method [32], the modified unified auxiliary equation [33], and many more have been developed for solving NLPDEs.

The present work aims to examine the $(1+1)$-dimensional Akbota equation (AE) (see [34]) given by

$$\begin{cases} iG_t + aG_{xx} + bG_{xt} + cGH = 0, \\ H_t - 2ad|G|_x^2 - 2bd|G|_t^2 = 0, \end{cases} \tag{1}$$

where $G = G(x,t)$ is a complex function, $H = H(x,t)$ is a real function and $d = \pm 1$. The coefficients a, b, and c represent arbitrary constants. The two equations above lead to particular models under suitable parametric scenarios. Notice, for example, that if $b = 0$, then the AE becomes the Schrödinger equation, and if $a = 0$, it becomes the Kuralay equation. Regarded as a Heisenberg ferromagnet-type equation, the AE is crucial for studying nonlinear phenomena in optics, curve and surface differential geometry, and magnets [34]. Analytical solutions for this equation are vital tools in both scientific inquiry and engineering practice. They not only provide a solid foundation for theoretical growth and enable accurate system control and prediction, but they also aid in the advancement of our understanding of the natural world. Given the wide range of scientific fields in which the AE finds application, analytical solutions are necessary to obtain insights of the model. Considering that analytical solutions provide for a complete understanding of the system's underlying behavior, as described by the equations. Their concise representation of the interactions between variables and parameters facilitates a deeper understanding of the underlying concepts driving the system.

The impetus for suggesting the Hirota bilinear method is the limitation of current approaches applied to the AE, including the Fan sub-equation method, Darboux transformation, and Lie

group method, which tend to fail in dealing with complicated wave interactions or deriving exact solutions for some nonlinear equations. Comprehensive solutions are required with the utmost urgency since the Hirota bilinear method is versatile in deriving various types of wave structures such as periodic, breather, and mixed waves, which are fundamental in explaining intricate nonlinear phenomena in areas of optics, magnetism, and differential geometry. Moreover, the ability of the method to generate physically sensible solutions that successfully simulate the dynamic characteristics of traveling-wave deformation fronts in dispersive media renders it a valuable asset for theoretical and experimental study. This accuracy and flexibility bridge gaps in existing approaches, gaining understanding of nonlinear system behavior at progressively deeper levels and driving applications throughout scientific and engineering disciplines.

This work is validated over current methods through the use of the Hirota bilinear technique, a established method for exact solutions of NLPDEs. The investigation obtained a variety of wave solutions such as periodic lump waves, periodic cross-kink waves, homoclinic breather waves, M-shaped waves, and mixed waves, proving the universality of the method. In comparison with findings from alternative approaches, such as the new extended auxiliary equation method, the Darboux transformation, modified Khater method, and Sardar sub-equation method, the versatility of the bilinear technique providing more complete and accurate results is emphasized. Precise graphical visualizations, viz., three-dimensional, contour, and density plots, are included to present physical structures and dynamical properties of the solutions in support of their accuracy. The research also completes some of the gaps in the existing literature, providing new insights to the solutions of the Akbota equation. The conformity of the results with well-established results of Painleve analysis and other methods, as well as their possible applications in surface geometry, nonlinear optics and magnetism, underscores the strength and applicability of the proposed method. Finally, this paper presents a number of important contributions to the research on the Heisenberg ferromagnet-type AE. Using the bilinear method, we obtained new wave solutions for this equation, such as periodic lump waves, homoclinic breathers, and M-shaped waves, which broaden the knowledge of nonlinear wave phenomena. The graphical solutions offer useful information on the dynamic nature of these waves, and the applicability of the solutions to practical problems lies in areas like nonlinear optics and magnetism. The study contributes to the theoretical development of the Akbota equation and proves the efficiency of the Hirota bilinear method in solving intricate systems.

2. Related works

This article explores solutions in the form of soliton waves for the AE with the use of the Hirota bilinear transformation technique. This approach is fundamental in the study of solitons and has been employed by numerous investigators such as Rizvi *et al.* [35], Ma *et al.* [36], Ma and Li [37], Khan and Wazwaz [38], Ahmed *et al.* [39], Ceesay *et al.* [40], Wang *et al.* [41], Yan *et al.* [42], Kumar and Mohan [43], Alsallami *et al.* [44] and many other researchers. These investigators were able to derive numerous wave solutions such as one and two solitons, lump, breather, periodic wave, cross kink, periodic cross kink, multiple wave, mixed waves, M-shaped waves and others. Recently, some reports have focused on the AE, and attempts have been made to address some of its important facets. For instance, by employing the new extended auxiliary equation method, Mathanaranjan and Myrzakulov [45] obtained Jacobi elliptic functions solutions in the forms of dark, bright, singular and singular periodic solitons in their limit conditions for the AE. Kong and Guo [46] used the J-fold Darboux transformation to explore this equation and were able extract one and two breather, rogue and semi-rational waves solutions.

Among other recent efforts [47, 48], Li and Zhao [49] examined the AE utilizing the analysis method of planar dynamic system. They obtained solitary wave solutions for this equation and also obtain the dynamic behavior of the two-dimensional dynamical system. By means

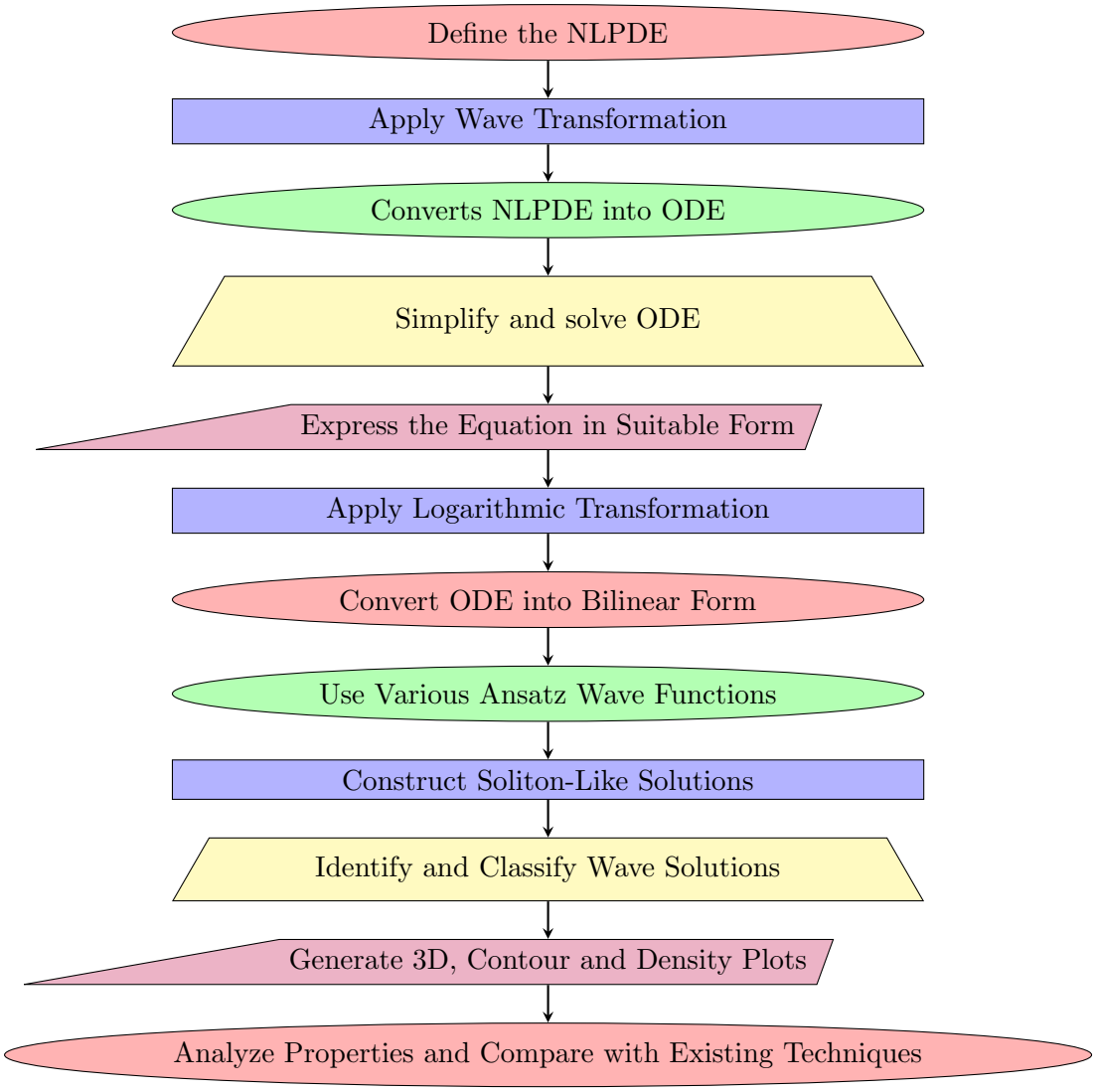

Figure 1: Flowchart of the methodology and solution derivation process.

of the modified Khater method and Sardar sub-equation method, Tariq *et al.* [50] studied the AE and obtained trigonometric, hyperbolic and rational functions solutions. They also studied the bifurcation and sensitivity analyses of the equation and showed that the chaotic system portrays both stable and unstable behaviors. In their work, Awadalla *et al.* [51] reached various forms of solutions for the AE such as bright, dark and periodic solitons, by employing numerous analytical techniques. Faridi *et al.* [52] applied different techniques to investigate this equation. They extracted solitons solutions such as dark, bright, singular, singular periodic, trigonometric, and hyperbolic waves. Still, there was a dearth of literature on a number of important and widespread forms of solitons for the AE. To close this gap, this work embark on establishing different sorts of novel solitons employing the Hirota bilinear transformation approach. To that end, the next section is devoted to recall briefly this methodology. The subsequent sections will report on particular types of solutions for the mathematical model under investigation.

3. Materials and methods

The Hirota bilinear transformation technique is a helpful tool in solving NLPDEs by transforming them into a bilinear equation. It also involved assuming ansatz wave functions in the form of exponential, polynomial, trigonometric, or hyperbolic functions and solving the derived

bilinear equations to obtain exact solutions. For the Heisenberg ferromagnet-type AE, the Hirota bilinear transformation is implemented by first converting the equation to an ODE via a wave transformation. The logarithmic transformation is utilized to transform the ODE to its bilinear form. The generated system is solved to derive wave solutions such as periodic lump waves, homoclinic breather waves, and M-shaped waves. The fact that the method provides accurate and physically relevant solutions explains why it is extremely useful to study complicated nonlinear phenomena in differential geometry, magnetism, and optics. The flowchart in Figure 1 outlines the step-by-step process of deriving wave solutions using the Hirota bilinear transformation technique.

The following steps are involved in the technique:

- **Step 1:** Consider NLPDE of the form

$$\begin{cases} M(GH, G, G_t, G_x, G_{xx}, H_x, \dots) = 0 \\ N(G_x, G_{xx}, H_x, \dots) = 0, \end{cases}, \tag{2}$$

  where $G = G(x,t)$ and $H = H(x,t)$ are the wave functions, x is a space variable and t is time.

- **Step 2:** To tranform the NLPDE to an ODE, we employ the wave transformation shown below.

$$\begin{aligned} G(x,t) &= \Lambda(\sigma)e^{i\tau}, \\ H(x,t) &= \Delta(\sigma), \\ \sigma &= x - \omega_1 t, \\ \tau &= -\theta x + \omega_2 t. \end{aligned} \tag{3}$$

  where wave velocity, frequency, and wave number are denoted by parameters ω_1, θ, and ω_2, respectively. Putting equation (3) into equation (2), reduces NLPDE to an ODE in terms of $\Lambda(\sigma)$ and $\Delta(\sigma)$.

- **Step 3:** To make the resulting ODE more tractable, integrate, rearrange, and substitute terms if required.

- **Step 4:** Applying the Cole-Hopf logarithmic transformation, we write $\Lambda(\sigma)$ in terms of a new function $\Phi(\sigma)$

$$\Lambda(\sigma) = R(ln(\Phi(\sigma))_\sigma, \tag{4}$$

  where R is a constant to be determined. Find the derivatives of $\Lambda(\sigma)$ (e.g. Λ', Λ'') in terms of $\Phi(\sigma)$ and its derivatives.

- **Step 5:** Replace $\Lambda(\sigma)$, $\Lambda'(\sigma)$, $\Lambda''(\sigma)$, etc. in the ODE of Equation (2). Rewrite the ODE in terms of $\Phi(\sigma)$ and its derivatives.

- **Step 6:** Express the ODE in bilinear form, which typically involves products of $\Phi(\sigma)$ and its derivatives.

- **Step 7:** Select the ansatz wave functions and input them into the bilinear equation for $\Phi(\sigma)$. Equate the coefficients of similar terms to zero to solve for the unknown parameters

- **Step 8:**After determining $\Phi(\sigma)$, use the Cole-Hopf logarithmic transformation in Equation (4) to recover $\Lambda(\sigma)$, and then get $\Delta(\sigma)$.

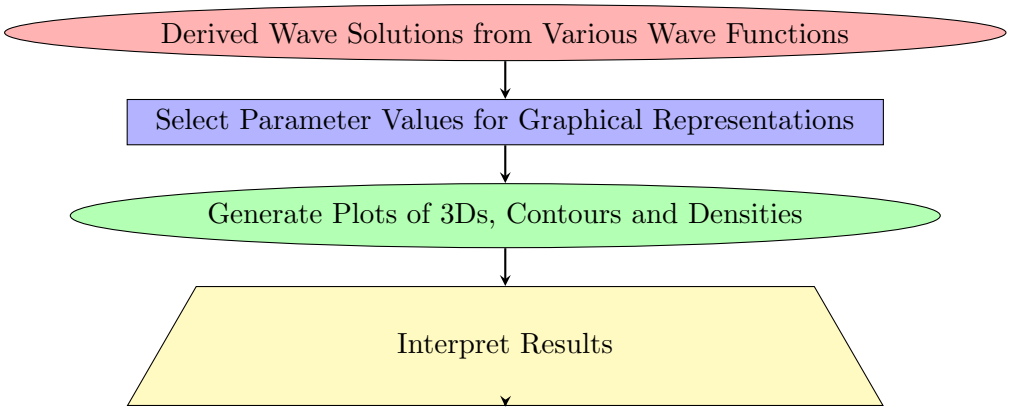

Figure 2: Flowchart of the graphical representation and analysis process.

- **Step 9:** In order to derive the solutions $G(x,t)$ and $H(x,t)$ in terms of the original variables, substitute the wave transformations in equation (3) into the solutions obtained in step 8.

The bilinear method is an efficient computational approach with easy steps such as conversion of the equation into bilinear form, taking an ansatz, and solving algebraic equations. This makes it well suited for finding exact solutions of an enormous number of NLPDEs. The bilinear method is also more efficient compared to current methods that use numerical methods for computations, which are extensive and yield only approximations. It is also more efficient than the Inverse scattering transform, which is based on the solution of intricate integral equations and spectral analysis. Although comparable in efficiency with methods such as the Fan sub-equation method and Darboux transformation, the efficiency of the bilinear method coupled with its ability to solve a wider class of equations and deliver exact solutions is a plus. Nonetheless, it may be difficult to obtain the bilinear form for some equations, a drawback of its efficiency and generality. Overall, the Hirota bilinear method finds an optimal balance between computational efficiency and generality, rendering it an effective tool in solving intricate NLPDEs. The flowchart in Figure 2 illustrates the process of analyzing and visualizing the derived wave solutions.

4. Results

For convenience, we will briefly recall now the Hirota bilinear methodology. We assume the following wave transformation solves Equation (1):

$$\begin{aligned} G(x,t) &= \Lambda(\sigma)e^{i\tau}, \\ H(x,t) &= \Delta(\sigma), \\ \sigma &= x - \omega_1 t, \\ \tau &= -\theta x + \omega_2 t. \end{aligned} \tag{5}$$

The soliton velocity, frequency, and wave number in this case are represented by the parameters ω_1, θ, and ω_2. However, the functions Λ and Δ of σ are what convert PDEs into ordinary differential Equations (ODEs). By employing Equation (5), we convert Equation (1) into the system of ODEs

$$\begin{cases} -i\omega_1\Lambda' - \omega_2\Lambda + a\Lambda'' - 2ia\theta\Lambda' - a\theta^2\Lambda - b\omega_1\Lambda'' \\ \qquad\qquad +ib\theta\omega_1\Lambda' + ib\omega_2\Lambda' + b\theta\omega_2\Lambda + c\Lambda\Delta = 0, \\ \Delta' - 4ad\Lambda\Lambda' + 4bd\omega_1\Lambda\Lambda' = 0. \end{cases} \tag{6}$$

In the first part of Equation (6), we separate the real and imaginary components accordingly to obtain

$$(b\omega_1 - a)\Lambda'' + (a\theta^2 + \omega_2 - b\theta\omega_2 - c\Delta)\Lambda = 0, \tag{7}$$

$$i(-\omega_1 - 2a\theta + b\theta\omega_1 + b\omega_2)\Lambda' = 0. \tag{8}$$

Integrate Equation (8) and solve for ω_2. At the same time, integrate the second part of Equation (6) and solve for Δ. As a consequence, we readily obtain that

$$\omega_2 = \frac{2a\theta + \omega_1 - b\theta\omega_1}{b}, \tag{9}$$

$$\Delta = 2d(a - b\omega_1)\Lambda^2. \tag{10}$$

Substituting Equations (9) and (10) into Equations (7), we reach

$$b(a - b\omega_1)\Lambda'' + (-\omega_1 + \theta(b\theta - 2)(a - b\omega_1))\Lambda + 2cd(a - b\omega_1)\Lambda^3 = 0. \tag{11}$$

We now use Equation (11) to find the various wave structures under consideration for Equation (1). We first assume that Equation (11) has a solution of the form

$$\Lambda(\sigma) = R(\ln(\Phi(\sigma))_\sigma, \tag{12}$$

where R is a constant to be determined. Substituting Equation (12) into Equation (11), we obtain

$$\begin{aligned} &2b\left(\Phi'\right)^3(a - b\omega_1)\left(cdR^2 + 1\right) \\ &+\Phi^2\left(\Phi'\left(a\theta(b\theta - 2) - \omega_1(b\theta - 1)^2\right) + b\Phi^{(3)}(a - b\omega_1)\right) \\ &+3b\Phi''\Phi\Phi'(b\omega_1 - a) = 0. \end{aligned} \tag{13}$$

We input the functions for the different wave types under investigation into Equation (13). Then, we expand, evaluate, and arrange related terms together, setting them equal to 0. Ultimately, we solve this system of equations to obtain a number of potential families for each instance. Various exact solutions for the Heisenberg ferromagnet-type Akbota will be derived in the following sections. At the end of each section, we will provide graphical representations of some typical solutions. The graphs will provide a clear representation of the soliton solutions found. Owing to the impact of graphical morphology on the dynamics of the traveling-wave solutions, we illustrate a range of solution types in (a) three-dimensional plots. Meanwhile, all subfigures (b) and (c) represent the contour plots while (d) and (e) depict the density plots. The contour plots help in visualizing the wave profiles by displaying changes in both shape and intensity in different spatial areas at different times. By displaying differences in wave density before and after interactions, density plots facilitate the analysis of the impact of collisions and the creation of new waves. These graphs also make parameter tuning and optimization easier because they illustrate how changes impact wave shape and density, which are crucial for optimizing parameters and system performance. Additionally, wave quality in a range of fields can be validated, compared, and optimized quantitatively using the contour and density plots.

4.1. Interaction of M-shaped with rogue and kink waves (MRK)

This wave configuration is provided by (see [53])

$$\Phi = J_2\exp(\sigma v_3 + v_4) + J_1\cosh(\sigma v_1 + v_2) + (\sigma v_5 + v_6)^2 + (\sigma v_7 + v_8)^2 + v_9. \tag{14}$$

By substituting Equation (14) and its first three derivatives into Equation (13), we obtain a simplified expression. We assemble similar terms together, and equate each expression's coefficients to zero. Thus, we obtain the following set of constant values.

Family 1.

$$v_1 = \frac{\sqrt{-ab\theta^2 + 2a\theta + b^2\theta^2\omega_1 - 2b\theta\omega_1 + \omega_1}}{\sqrt{2b^2\omega_1 - 2ab}},$$

$$v_3 = -\frac{\sqrt{-ab\theta^2 + 2a\theta + b^2\theta^2\omega_1 - 2b\theta\omega_1 + \omega_1}}{\sqrt{2b^2\omega_1 - 2ab}},$$

$$v_5 = 0,$$

$$v_7 = 0,$$

$$v_9 = -v_6^2 - v_8^2.$$

Inserting these values into Equation (14) and then the result in Equation (12), we have

$$\Lambda_{1MRK}(\sigma) = \frac{i\sqrt{a\theta(2-b\theta)+\omega_1(b\theta-1)^2}\left(J_1\left(\exp\left(\frac{\sigma\sqrt{2\omega_1(b\theta-1)^2-2a\theta(b\theta-2)}}{\sqrt{b(b\omega_1-a)}}+2v_2\right)-1\right)-2J_2e^{v_2+v_4}\right)}{\sqrt{2}\sqrt{c}\sqrt{d}\sqrt{b\left(b\omega_1-a\right)}\left(J_1\left(\exp\left(\frac{\sigma\sqrt{2\omega_1(b\theta-1)^2-2a\theta(b\theta-2)}}{\sqrt{b(b\omega_1-a)}}+2v_2\right)+1\right)+2J_2e^{v_2+v_4}\right)}. \tag{15}$$

Substituting Equation (15) into Equation (10) gives

$$\Delta_{1MRK}(\sigma) = \frac{\left(a\theta(2-b\theta)+\omega_1(b\theta-1)^2\right)\left(J_1\left(\exp\left(\frac{\sigma\sqrt{2\omega_1(b\theta-1)^2-2a\theta(b\theta-2)}}{\sqrt{b(b\omega_1-a)}}+2v_2\right)-1\right)-2J_2e^{v_2+v_4}\right)^2}{bc\left(J_1\left(\exp\left(\frac{\sigma\sqrt{2\omega_1(b\theta-1)^2-2a\theta(b\theta-2)}}{\sqrt{b(b\omega_1-a)}}+2v_2\right)+1\right)+2J_2e^{v_2+v_4}\right)^2}. \tag{16}$$

Substituting Equations (15) and (16) into Equation (5) yields the required MRK wave solutions for Equation (1):

$$G_{1MRK}(x,t) = \frac{i\left(\left(A_1-1\right)J_1-2J_2e^{v_2+v_4}\right)\sqrt{a\theta(2-b\theta)+\omega_1(b\theta-1)^2}\exp\left(\frac{i(\theta(2at-bx)+\omega_1(t-b\theta t))}{b}\right)}{\sqrt{2}\sqrt{c}\sqrt{d}\sqrt{b\left(b\omega_1-a\right)}\left(\left(A_1+1\right)J_1+2J_2e^{v_2+v_4}\right)}, \tag{17}$$

$$H_{1MRK}(x,t) = \frac{\left(\left(A_1-1\right)J_1-2J_2e^{v_2+v_4}\right)^2\left(a\theta(2-b\theta)+\omega_1(b\theta-1)^2\right)}{bc\left(\left(A_1+1\right)J_1+2J_2e^{v_2+v_4}\right)^2}. \tag{18}$$

Here,

$$A_1 = \exp\left(\frac{\left(x-t\omega_1\right)\sqrt{2\omega_1(b\theta-1)^2-2a\theta(b\theta-2)}}{\sqrt{b\left(b\omega_1-a\right)}}+2v_2\right). \tag{19}$$

For illustration purposes, Figures 3 and 4 show M-shaped waves obtained from an interaction between M-shaped with rogue and kink waves. In particular, Figure 3 depicts the solution $G_{1MRK}(x,t)$ corresponding to Equation 17 for the parameter values $v_2 = 2.7$, $v_4 = 1.7$, $J_1 = 0.4$, $J_2 = 2.6$, $a = 5.1$, $b = 3.1$, $c = 5.2$, $d = 1$, $\omega_1 = 0.1$ and $\theta = 0.1$. Figure 4 is obtained from the solution $H_{1MRK}(x,t)$ corresponding to Equation 18, for the same parameter values.

4.2. Multi waves (MU)

This pattern of waves is derived from (see [54])

$$\Phi = J_2\cos\left(k\left(\sigma v_3+v_4\right)\right)+J_1\cosh\left(k\left(\sigma v_1+v_2\right)\right)+J_3\cosh\left(k\left(\sigma v_5+v_6\right)\right). \tag{20}$$

Proceeding as in the previous section, we readily obtain the following sets of constant values:

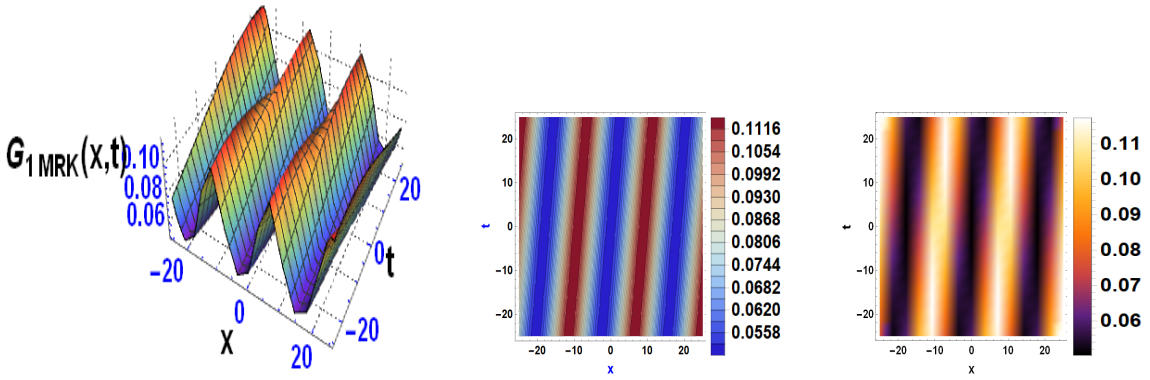

(a) (b) (c)

Figure 3: (a) Three-dimensional plot, (b) contour plot and (c) density plot corresponding to the function G_{1MRK} versus x and t. We used the parameters $v_2 = 2.7$, $v_4 = 1.7$, $J_1 = 0.4$, $J_2 = 2.6$, $a = 5.1$, $b = 3.1$, $c = 5.2$, $d = 1$, $\omega_1 = 0.1$ and $\theta = 0.1$.

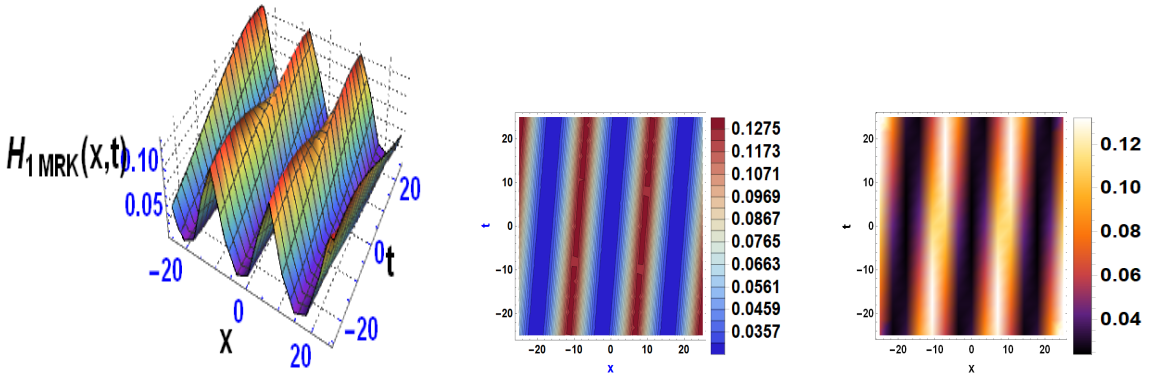

(a) (b) (c)

Figure 4: (a) Three-dimensional plot, (b) contour plot and (c) density plot corresponding to the function H_{1MRK} versus x and t. We used the parameters $v_2 = 2.7$, $v_4 = 1.7$, $J_1 = 0.4$, $J_2 = 2.6$, $a = 5.1$, $b = 3.1$, $c = 5.2$, $d = 1$, $\omega_1 = 0.1$ and $\theta = 0.1$.

Family 1.

$$J_1 = 0,$$

$$v_3 = \frac{\sqrt{-ab\theta^2 + 2a\theta + b^2\theta^2\omega_1 - 2b\theta\omega_1 + \omega_1}}{\sqrt{2}\sqrt{abk^2 - b^2k^2\omega_1}},$$

$$v_5 = -\frac{\sqrt{-ab\theta^2 + 2a\theta + b^2\theta^2\omega_1 - 2b\theta\omega_1 + \omega_1}}{\sqrt{2b^2k^2\omega_1 - 2abk^2}},$$

$$R = -\frac{i}{\sqrt{c}\sqrt{d}}.$$

Substituting them into Equation (20) and then the outcome in Equation (12), we have

$$\Lambda_{1MU}(\sigma) = \frac{ik\sqrt{a\theta(2-b\theta)+\omega_1(b\theta-1)^2}\left(J_2\sin(A_3k)\sqrt{bk^2(b\omega_1-a)}+J_3\sinh(A_2k)\sqrt{bk^2(a-b\omega_1)}\right)}{\sqrt{2}\sqrt{c}\sqrt{d}\sqrt{-b^2k^4(a-b\omega_1)^2}\left(J_2\cos(A_3k)+J_3\cosh(A_2k)\right)}. \tag{21}$$

Substituting Equation (21) into Equation (10) yields

$$\Delta_{1MU}(\sigma) = \frac{\left(a\theta(b\theta-2)-\omega_1(b\theta-1)^2\right)\left(J_2\sin(A_3k)\sqrt{bk^2(b\omega_1-a)}+J_3\sinh(A_2k)\sqrt{bk^2(a-b\omega_1)}\right)^2}{b^2ck^2(b\omega_1-a)\left(J_2\cos(A_3k)+J_3\cosh(A_2k)\right)^2}, \tag{22}$$

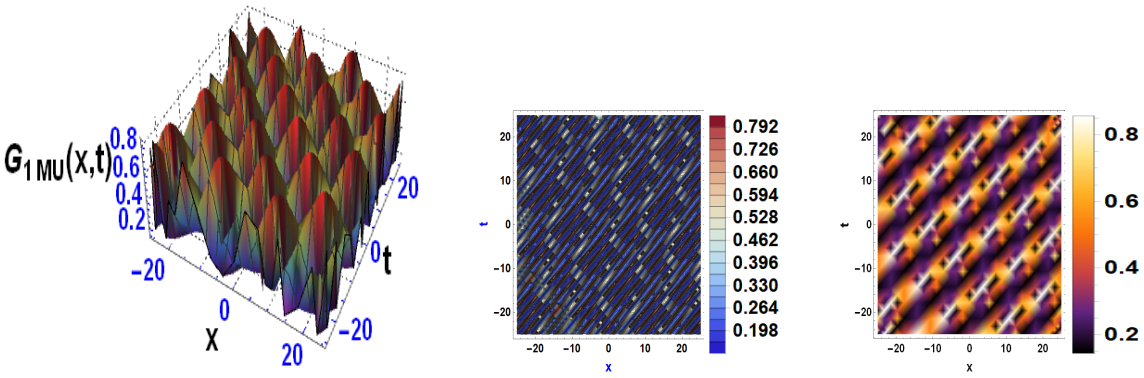

(a) (b) (c)

Figure 5: (a) Three-dimensional plot, (b) contour plot and (c) density plot corresponding to the function G_{1MU} versus x and t. We used the parameters $v_4 = 5.1$, $v_6 = 6.7$, $J_2 = 4.6$, $J_3 = 8.4$, $a = 4.4$, $b = 0.7$, $c = 8.9$, $d = 1$, $k = 0.1$, $\omega_1 = 1.1$ and $\theta = 0.9$.

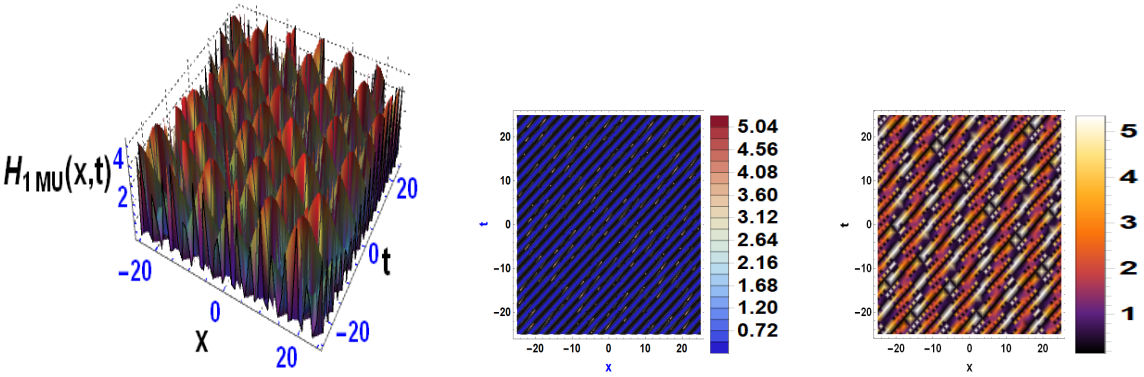

(a) (b) (c)

Figure 6: (a) Three-dimensional plot, (b) contour plot and (c) density plot corresponding to the function H_{1MU} versus x and t. We used the parameters $v_4 = 5.1$, $v_6 = 6.7$, $J_2 = 4.6$, $J_3 = 8.4$, $a = 4.4$, $b = 0.7$, $c = 8.9$, $d = 1$, $k = 0.1$, $\omega_1 = 1.1$ and $\theta = 0.9$.

where

$$A_2 = v_6 - \frac{\sigma\sqrt{a\theta(2-b\theta)+\omega_1(b\theta-1)^2}}{\sqrt{2}\sqrt{bk^2\,(b\omega_1-a)}}, \tag{23}$$

$$A_3 = \frac{\sigma\sqrt{a\theta(2-b\theta)+\omega_1(b\theta-1)^2}}{\sqrt{2}\sqrt{bk^2\,(a-b\omega_1)}} + v_4. \tag{24}$$

Substituting Equations (21) and (22) into Equation (5) gives the MU wave solutions for Equation (1):

$$G_{1MU}(x,t) = \frac{iA_6k\sqrt{a\theta(2-b\theta)+\omega_1(b\theta-1)^2}\left(J_2\sin(A_5k)\sqrt{bk^2(b\omega_1-a)}+J_3\sinh(A_4k)\sqrt{bk^2(a-b\omega_1)}\right)}{\sqrt{2}\sqrt{c}\sqrt{d}\sqrt{-b^2k^4(a-b\omega_1)^2}(J_2\cos(A_5k)+J_3\cosh(A_4k))}, \tag{25}$$

$$H_{1MU}(x,t) = \frac{\left(a\theta(b\theta-2)-\omega_1(b\theta-1)^2\right)\left(J_2\sin(A_5k)\sqrt{bk^2(b\omega_1-a)}+J_3\sinh(A_4k)\sqrt{bk^2(a-b\omega_1)}\right)^2}{b^2ck^2(b\omega_1-a)(J_2\cos(A_5k)+J_3\cosh(A_4k))^2}, \tag{26}$$

where

$$A_4 = \frac{(t\omega_1-x)\sqrt{a\theta(2-b\theta)+\omega_1(b\theta-1)^2}}{\sqrt{2}\sqrt{bk^2\,(b\omega_1-a)}} + v_6, \tag{27}$$

$$A_5 = \frac{(x-t\omega_1)\sqrt{a\theta(2-b\theta)+\omega_1(b\theta-1)^2}}{\sqrt{2}\sqrt{bk^2\,(a-b\omega_1)}} + v_4, \tag{28}$$

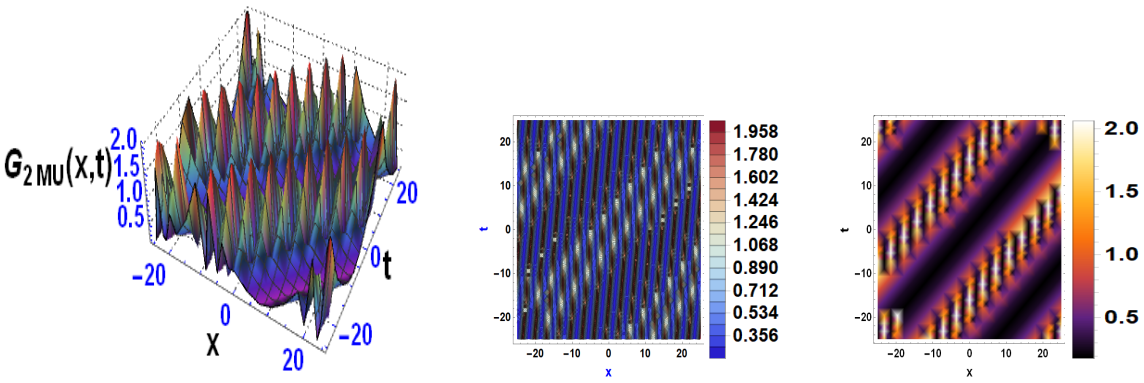

(a) (b) (c)

Figure 7: (a) Three-dimensional plot, (b) contour plot and (c) density plot corresponding to the function G_{2MU} versus x and t. We used the parameters $v_2 = 9.0$, $v_4 = 7.4$, $v_6 = 9.3$, $J_1 = 2.5$, $J_2 = 0.9$, $J_3 = 1.6$, $a = 4.0$, $b = 0.4$, $c = 2.6$, $d = 1$, $k = 3.5$, $\omega_1 = 0.1$ and $\theta = 0.4$.

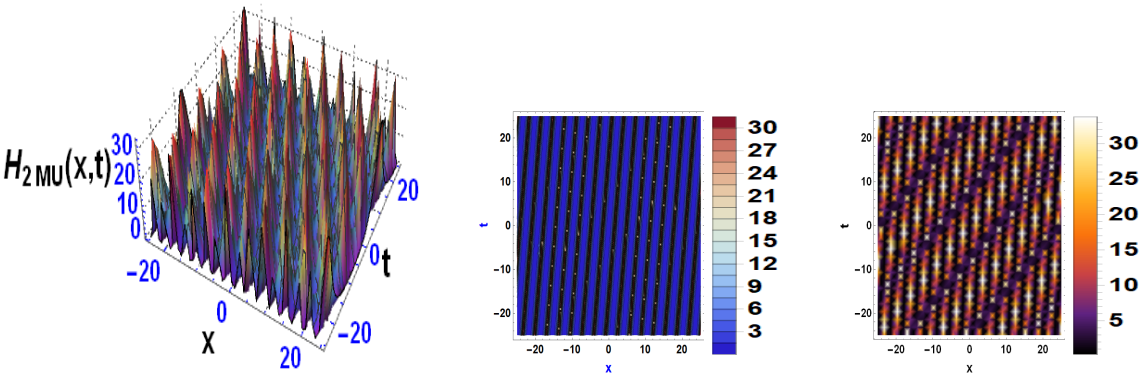

(a) (b) (c)

Figure 8: (a) Three-dimensional plot, (b) contour plot and (c) density plot corresponding to the function H_{2MU} versus x and t. We used the parameters $v_2 = 9.0$, $v_4 = 7.4$, $v_6 = 9.3$, $J_1 = 2.5$, $J_2 = 0.9$, $J_3 = 1.6$, $a = 4.0$, $b = 0.4$, $c = 2.6$, $d = 1$, $k = 3.5$, $\omega_1 = 0.1$ and $\theta = 0.4$.

$$A_6 = \exp\left(-\frac{i\left(-2a\theta t + t\omega_1(b\theta - 1) + b\theta x\right)}{b}\right). \tag{29}$$

Family 2.

$$v_1 = \frac{\sqrt{-ab\theta^2 + 2a\theta + b^2\theta^2\omega_1 - 2b\theta\omega_1 + \omega_1}}{\sqrt{2b^2k^2\omega_1 - 2abk^2}},$$

$$v_3 = \frac{\sqrt{-ab\theta^2 + 2a\theta + b^2\theta^2\omega_1 - 2b\theta\omega_1 + \omega_1}}{\sqrt{2}\sqrt{abk^2 - b^2k^2\omega_1}},$$

$$v_5 = -\frac{\sqrt{-ab\theta^2 + 2a\theta + b^2\theta^2\omega_1 - 2b\theta\omega_1 + \omega_1}}{\sqrt{2b^2k^2\omega_1 - 2abk^2}},$$

$$R = \frac{i}{\sqrt{c}\sqrt{d}}.$$

Substituting into Equation (20) and then the result into Equation (12), we reach

$$\Lambda_{2MU}(\sigma) = -\frac{ik\sqrt{a\theta(2-b\theta)+\omega_1(b\theta-1)^2}\left(J_2\sin(A_3k)\sqrt{bk^2(b\omega_1-a)}+\sqrt{bk^2(a-b\omega_1)}(J_3\sinh(A_2k)-J_1\sinh(A_7k))\right)}{\sqrt{2}\sqrt{c}\sqrt{d}\sqrt{-b^2k^4(a-b\omega_1)^2}(J_2\cos(A_3k)+J_1\cosh(A_7k)+J_3\cosh(A_2k))}. \tag{30}$$

Substituting Equation (30) into Equation (10) gives

$$\Delta_{2MU}(\sigma) = \frac{\left(a\theta(b\theta-2)-\omega_1(b\theta-1)^2\right)\left(J_2\sin(A_3k)\sqrt{bk^2(b\omega_1-a)}+\sqrt{bk^2(a-b\omega_1)}(J_3\sinh(A_2k)-J_1\sinh(A_7k))\right)^2}{b^2ck^2(b\omega_1-a)(J_2\cos(A_3k)+J_1\cosh(A_7k)+J_3\cosh(A_2k))^2}, \tag{31}$$

where

$$A_7 = \frac{\sigma\sqrt{a\theta(2-b\theta)+\omega_1(b\theta-1)^2}}{\sqrt{2}\sqrt{bk^2\left(b\omega_1-a\right)}} + v_2. \tag{32}$$

Applying Equations (30) and (31) into Equation (5) gives the MU wave solutions for Equation (1), namely,

$$G_{2MU}(x,t) = -\frac{iA_6k\sqrt{a\theta(2-b\theta)+\omega_1(b\theta-1)^2}\left(J_2\sin(A_5k)\sqrt{bk^2(b\omega_1-a)}+\sqrt{bk^2(a-b\omega_1)}(J_3\sinh(A_4k)-J_1\sinh(A_8k))\right)}{\sqrt{2}\sqrt{c}\sqrt{d}\sqrt{-b^2k^4(a-b\omega_1)^2}(J_2\cos(A_5k)+J_1\cosh(A_8k)+J_3\cosh(A_4k))}, \tag{33}$$

$$H_{2MU}(x,t) = \frac{\left(a\theta(b\theta-2)-\omega_1(b\theta-1)^2\right)\left(J_2\sin(A_5k)\sqrt{bk^2(b\omega_1-a)}+\sqrt{bk^2(a-b\omega_1)}(J_3\sinh(A_4k)-J_1\sinh(A_8k))\right)^2}{b^2ck^2(b\omega_1-a)(J_2\cos(A_5k)+J_1\cosh(A_8k)+J_3\cosh(A_4k))^2}, \tag{34}$$

where

$$A_8 = \frac{(x-t\omega_1)\sqrt{a\theta(2-b\theta)+\omega_1(b\theta-1)^2}}{\sqrt{2}\sqrt{bk^2\left(b\omega_1-a\right)}} + v_2. \tag{35}$$

For the sake of convenience, Figures 5 and 6 portray multiple bright breather-like waves arising from the wave structure function of multi waves. Using the solution $G_{1MU}(x,t)$ corresponding to Equation (25), we obtained Figure 5 by selecting the parameter values $v_4 = 5.1$, $v_6 = 6.7$, $J_2 = 4.6$, $J_3 = 8.4$, $a = 4.4$, $b = 0.7$, $c = 8.9$, $d = 1$, $k = 0.1$, $\omega_1 = 1.1$ and $\theta = 0.9$. The solution $H_{1MU}(x,t)$ corresponding to Equation (26) is shown in Figure 6 for the same choice of parameter values as for Figure 5. On the other hand, Figure 7 was obtained using Equation (33) with parameter values $v_2 = 9.0$, $v_4 = 7.4$, $v_6 = 9.3$, $J_1 = 2.5$, $J_2 = 0.9$, $J_3 = 1.6$, $a = 4.0$, $b = 0.4$, $c = 2.6$, $d = 1$, $k = 3.5$, $\omega_1 = 0.1$ and $\theta = 0.4$. The solution $H_{2MU}(x,t)$ corresponding to Equation (34) is shown in Figure 8.

4.3. Periodic lump (PL)

This wave structure is derived by using (see [54])

$$\Phi(\sigma) = (\sigma v_1 + v_2)^2 + (\sigma v_3 + v_4)^2 + \cos(\sigma v_5 + v_6) + v_7. \tag{36}$$

Substitute Equation (36) and its first three derivatives into Equation (13). Proceeding as before, we derive the following set of constant values:

Family 1.

$$v_1 = iv_3,$$

$$v_4 = -iv_2,$$

$$v_5 = \frac{\sqrt{-ab\theta^2+2a\theta+b^2\theta^2\omega_1-2b\theta\omega_1+\omega_1}}{\sqrt{2}\sqrt{ab-b^2\omega_1}},$$

$$v_7 = 0,$$

$$R = \frac{i}{\sqrt{c}\sqrt{d}}.$$

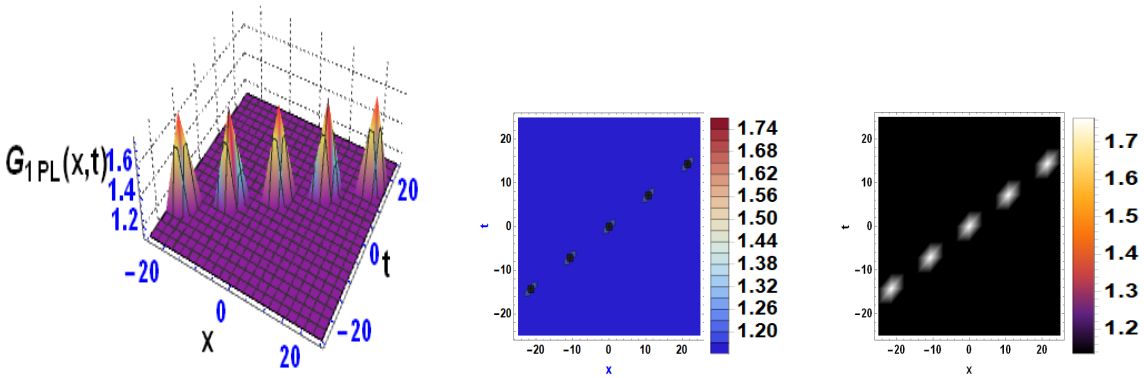

(a) (b) (c)

Figure 9: (a) Three-dimensional plot, (b) contour plot and (c) density plot corresponding to the function G_{1PL} versus x and t. We used the parameters $v_6 = 1.4$, $a = 1.5$, $b = 6.9$, $c = 3.4$, $d = 1$, $\omega_1 = 1.5$, $\theta = 3.1$.

By replacing them into Equation (36) and the outcome into Equation (12), we obtain

$$\Lambda_{1PL}(\sigma) = -\frac{i\sqrt{a\theta(2-b\theta)+\omega_1(b\theta-1)^2}\tan\left(\frac{\sigma\sqrt{a\theta(2-b\theta)+\omega_1(b\theta-1)^2}}{\sqrt{2}\sqrt{b(a-b\omega_1)}}+v_6\right)}{\sqrt{2}\sqrt{c}\sqrt{d}\sqrt{b\,(a-b\omega_1)}}. \tag{37}$$

Substituting Equation (37) into Equation (10) yields

$$\Delta_{1PL}(\sigma) = \frac{\left(a\theta(b\theta-2)-\omega_1(b\theta-1)^2\right)\tan^2\left(\frac{\sigma\sqrt{a\theta(2-b\theta)+\omega_1(b\theta-1)^2}}{\sqrt{2}\sqrt{b(a-b\omega_1)}}+v_6\right)}{bc}. \tag{38}$$

Substituting Equations (37) and (38) into Equation (5) gives PL wave solutions for Equation (1):

$$G_{1PL}(x,t) = -\frac{i\sqrt{a\theta(2-b\theta)+\omega_1(b\theta-1)^2}\exp\left(-\frac{i(-2a\theta t+t\omega_1(b\theta-1)+b\theta x)}{b}\right)\tan\left(\frac{(x-t\omega_1)\sqrt{a\theta(2-b\theta)+\omega_1(b\theta-1)^2}}{\sqrt{2}\sqrt{b(a-b\omega_1)}}+v_6\right)}{\sqrt{2}\sqrt{c}\sqrt{d}\sqrt{b(a-b\omega_1)}}, \tag{39}$$

$$H_{1PL}(x,t) = \frac{\left(a\theta(b\theta-2)-\omega_1(b\theta-1)^2\right)\tan^2\left(\frac{(x-t\omega_1)\sqrt{a\theta(2-b\theta)+\omega_1(b\theta-1)^2}}{\sqrt{2}\sqrt{b(a-b\omega_1)}}+v_6\right)}{bc}, \tag{40}$$

Figures 9 and 10 depict multiple periodic bright lump-like wave solutions. In particular, Figure 9 shows the solution $G_{1LP}(x,t)$ corresponding to Equation (39) for the parameters $v_6 = 1.4$, $a = 1.5$, $b = 6.9$, $c = 3.4$, $d = 1$, $\omega_1 = 1.5$, $\theta = 3.1$. Meanwhile, Figure 10 shows the solution $H_{1LP}(x,t)$ provided by Equation (40) for the same choice of parameter values.

4.4. Periodic cross kink (PCK)

This pattern of waves is reached by using (see [54])

$$\Phi(\sigma) = J_1\exp\left(k\left(\sigma v_3+v_4\right)\right)+\exp\left(-k\left(\sigma v_1+v_2\right)\right)+J_2\cos\left(k\left(\sigma v_5+v_6\right)\right)+J_3\cosh\left(k\left(\sigma v_7+v_8\right)\right)+v_9. \tag{41}$$

By substituting Equation (41) and its first three derivatives into Equation (13), and proceeding as before, we derive the following sets of constant values:

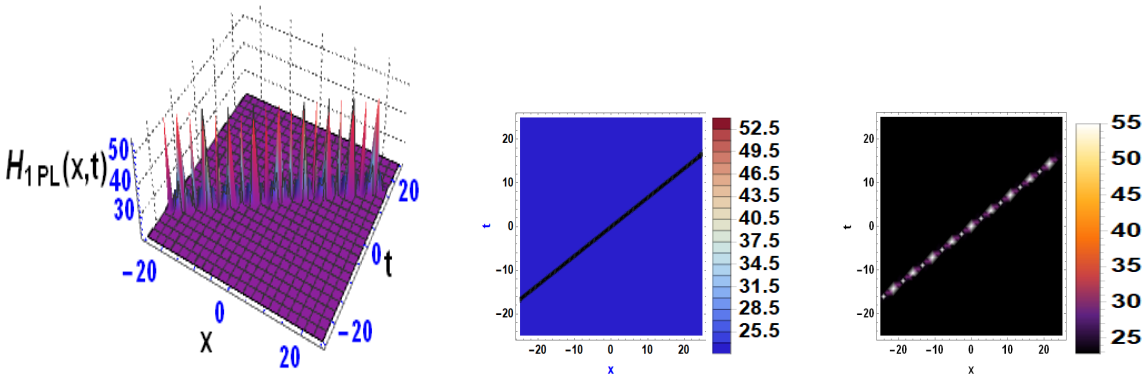

(a) (b) (c)

Figure 10: (a) Three-dimensional plot, (b) contour plot and (c) density plot corresponding to the function H_{1PL} versus x and t. We used the parameters $v_6 = 1.4$, $a = 1.5$, $b = 6.9$, $c = 3.4$, $d = 1$, $\omega_1 = 1.5$, $\theta = 3.1$.

Family 1.

$$J_3 = 0,$$

$$v_1 = -\frac{\sqrt{-ab\theta^2 + 2a\theta + b^2\theta^2\omega_1 - 2b\theta\omega_1 + \omega_1}}{\sqrt{2}\sqrt{-bk^2\,(a - b\omega_1)}},$$

$$v_3 = -\frac{\sqrt{-ab\theta^2 + 2a\theta + b^2\theta^2\omega_1 - 2b\theta\omega_1 + \omega_1}}{\sqrt{2b^2k^2\omega_1 - 2abk^2}},$$

$$v_5 = -\frac{\sqrt{-ab\theta^2 + 2a\theta + b^2\theta^2\omega_1 - 2b\theta\omega_1 + \omega_1}}{\sqrt{2}\sqrt{abk^2 - b^2k^2\omega_1}},$$

$$v_9 = 0,$$

$$R = \frac{i}{\sqrt{c}\sqrt{d}}.$$

Substituting these constant values into Equation (41) and then the outcome into Equation (12), we reach

$$\Lambda_{1PCK}(\sigma) = -\left(\frac{ik\sqrt{a\theta(2-b\theta)+\omega_1(b\theta-1)^2}\left(J_1\sqrt{bk^2(a-b\omega_1)}\exp\left(k\left(-\frac{\sigma\sqrt{2\omega_1(b\theta-1)^2-2a\theta(b\theta-2)}}{\sqrt{bk^2(b\omega_1-a)}}+v_2+v_4\right)\right)-\sqrt{bk^2(a-b\omega_1)}-A_9\right)}{\sqrt{2}\sqrt{c}\sqrt{d}\left(J_1\exp\left(k\left(-\frac{\sigma\sqrt{2\omega_1(b\theta-1)^2-2a\theta(b\theta-2)}}{\sqrt{bk^2(b\omega_1-a)}}+v_2+v_4\right)\right)+A_{10}+1\right)}\right). \tag{42}$$

Substituting Equation (42) into Equation (10) yields

$$\Delta_{1PCK}(\sigma) = -\frac{\left(a\theta(2-b\theta)+\omega_1(b\theta-1)^2\right)\left(J_1\sqrt{bk^2(a-b\omega_1)}\left(-\exp\left(k\left(-\frac{\sigma\sqrt{2\omega_1(b\theta-1)^2-2a\theta(b\theta-2)}}{\sqrt{bk^2(b\omega_1-a)}}+v_2+v_4\right)\right)\right)+\sqrt{bk^2(a-b\omega_1)}+A_9\right)^2}{bc\left(J_1\exp\left(k\left(-\frac{\sigma\sqrt{2\omega_1(b\theta-1)^2-2a\theta(b\theta-2)}}{\sqrt{bk^2(b\omega_1-a)}}+v_2+v_4\right)\right)+A_{10}+1\right)^2}, \tag{43}$$

where

$$\begin{aligned} A_9 = {} & J_2\sqrt{bk^2\,(b\omega_1 - a)}\exp\left(k\left(v_2 - \frac{\sigma\sqrt{a\theta(2-b\theta)+\omega_1(b\theta-1)^2}}{\sqrt{2}\sqrt{bk^2\,(b\omega_1-a)}}\right)\right) \\ & \cdot\sin\left(k\left(v_6 - \frac{\sigma\sqrt{a\theta(2-b\theta)+\omega_1(b\theta-1)^2}}{\sqrt{2}\sqrt{bk^2\,(a-b\omega_1)}}\right)\right) \end{aligned} \tag{44}$$

and

$$\begin{aligned} A_{10} = J_2 \exp\left(k\left(v_2 - \frac{\sigma\sqrt{a\theta(2-b\theta)+\omega_1(b\theta-1)^2}}{\sqrt{2}\sqrt{bk^2\left(b\omega_1-a\right)}}\right)\right) \\ \cdot \cos\left(k\left(v_6 - \frac{\sigma\sqrt{a\theta(2-b\theta)+\omega_1(b\theta-1)^2}}{\sqrt{2}\sqrt{bk^2\left(a-b\omega_1\right)}}\right)\right)\sqrt{-b^2k^4\left(a-b\omega_1\right)^2}. \end{aligned} \tag{45}$$

Substituting Equations (42) and (43) into Equation (5) gives a PCK wave solutions for Equation (1):

$$G_{1PCK}(x,t) = \frac{iA_{13}\left(J_1\sqrt{bk^2(a-b\omega_1)}\left(-\exp\left(k\left(\frac{(t\omega_1-x)\sqrt{2\omega_1(b\theta-1)^2-2a\theta(b\theta-2)}}{\sqrt{bk^2(b\omega_1-a)}}+v_2+v_4\right)\right)\right)+\sqrt{bk^2(a-b\omega_1)}+A_{11}\right)}{\sqrt{2}\sqrt{c}\sqrt{d}\left(J_1\exp\left(k\left(\frac{(t\omega_1-x)\sqrt{2\omega_1(b\theta-1)^2-2a\theta(b\theta-2)}}{\sqrt{bk^2(b\omega_1-a)}}+v_2+v_4\right)\right)+A_{12}+1\right)}, \tag{46}$$

$$H_{1PCK}(x,t) = -\frac{\left(a\theta(2-b\theta)+\omega_1(b\theta-1)^2\right)\left(J_1\sqrt{bk^2(a-b\omega_1)}\left(-\exp\left(k\left(\frac{(t\omega_1-x)\sqrt{2\omega_1(b\theta-1)^2-2a\theta(b\theta-2)}}{\sqrt{bk^2(b\omega_1-a)}}+v_2+v_4\right)\right)\right)+\sqrt{bk^2(a-b\omega_1)}+A_{11}\right)^2}{bc\left(J_1\exp\left(k\left(\frac{(t\omega_1-x)\sqrt{2\omega_1(b\theta-1)^2-2a\theta(b\theta-2)}}{\sqrt{bk^2(b\omega_1-a)}}+v_2+v_4\right)\right)+A_{12}+1\right)^2}, \tag{47}$$

where

$$\begin{aligned} A_{11} = J_2\sqrt{bk^2\left(b\omega_1-a\right)}\exp\left(k\left(\frac{\left(t\omega_1-x\right)\sqrt{a\theta(2-b\theta)+\omega_1(b\theta-1)^2}}{\sqrt{2}\sqrt{bk^2\left(b\omega_1-a\right)}}+v_2\right)\right) \\ \cdot \sin\left(k\left(\frac{\left(t\omega_1-x\right)\sqrt{a\theta(2-b\theta)+\omega_1(b\theta-1)^2}}{\sqrt{2}\sqrt{bk^2\left(a-b\omega_1\right)}}+v_6\right)\right), \end{aligned} \tag{48}$$

$$\begin{aligned} A_{12} = J_2\sqrt{-b^2k^4\left(a-b\omega_1\right)^2}\exp\left(k\left(\frac{\left(t\omega_1-x\right)\sqrt{a\theta(2-b\theta)+\omega_1(b\theta-1)^2}}{\sqrt{2}\sqrt{bk^2\left(b\omega_1-a\right)}}+v_2\right)\right) \\ \cdot \cos\left(k\left(\frac{\left(t\omega_1-x\right)\sqrt{a\theta(2-b\theta)+\omega_1(b\theta-1)^2}}{\sqrt{2}\sqrt{bk^2\left(a-b\omega_1\right)}}+v_6\right)\right) \end{aligned} \tag{49}$$

and

$$A_{13} = k\sqrt{a\theta(2-b\theta)+\omega_1(b\theta-1)^2}\exp\left(-\frac{i\left(-2a\theta t+t\omega_1(b\theta-1)+b\theta x\right)}{b}\right). \tag{50}$$

Family 2.

$$\begin{aligned} J_2 &= 0, \\ v_1 &= \frac{\sqrt{-ab\theta^2+2a\theta+b^2\theta^2\omega_1-2b\theta\omega_1+\omega_1}}{\sqrt{2b^2k^2\omega_1-2abk^2}}, \\ v_3 &= \frac{\sqrt{-ab\theta^2+2a\theta+b^2\theta^2\omega_1-2b\theta\omega_1+\omega_1}}{\sqrt{2b^2k^2\omega_1-2abk^2}}, \\ v_7 &= \frac{\sqrt{-ab\theta^2+2a\theta+b^2\theta^2\omega_1-2b\theta\omega_1+\omega_1}}{\sqrt{2b^2k^2\omega_1-2abk^2}}, \\ v_9 &= 0, \\ R &= \frac{i}{\sqrt{c}\sqrt{d}}. \end{aligned}$$

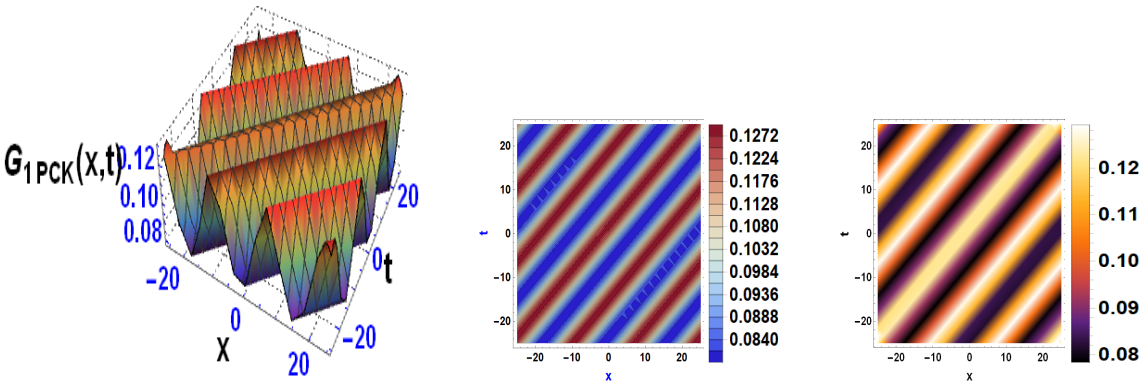

(a) (b) (c)

Figure 11: (a) Three-dimensional plot, (b) contour plot and (c) density plot corresponding to the function G_{1PCK} versus x and t. We used the parameters $v_2 = 0.4$, $v_4 = 0.8$, $v_6 = 2.3$, $J_1 = 9.1$, $J_2 = 5.9$, $J_4 = 1.2$, $a = 9.1$, $b = 5.0$, $c = 3.5$, $d = 1$, $k = 1.1$, $\omega_1 = 0.99$ and $\theta = 0.33$.

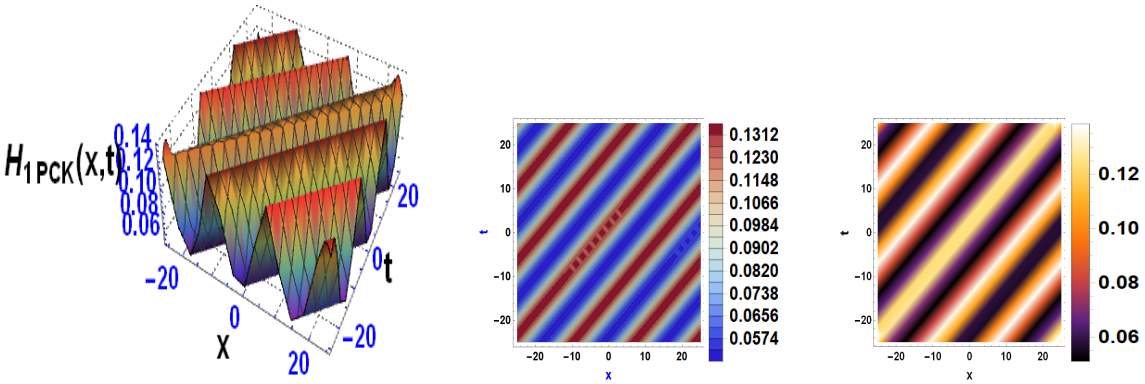

(a) (b) (c)

Figure 12: (a) Three-dimensional plot, (b) contour plot and (c) density plot corresponding to the function H_{1PCK} versus x and t. We used the parameters $v_2 = 0.4$, $v_4 = 0.8$, $v_6 = 2.3$, $J_1 = 9.1$, $J_2 = 5.9$, $J_4 = 1.2$, $a = 9.1$, $b = 5.0$, $c = 3.5$, $d = 1$, $k = 1.1$, $\omega_1 = 0.99$ and $\theta = 0.33$.

Substituting these values into Equation (41) and then the result into Equation (12), we have

$$\Lambda_{2PCK}(\sigma) = \frac{ik\left(J_1 \exp\left(k\left(\frac{\sigma\sqrt{2\omega_1(b\theta-1)^2-2a\theta(b\theta-2)}}{\sqrt{bk^2(b\omega_1-a)}} + v_2 + v_4\right)\right) + A_{14} - 1\right)}{\sqrt{2}\sqrt{c}\sqrt{d}\left(J_1 \exp\left(k\left(\frac{\sigma\sqrt{2\omega_1(b\theta-1)^2-2a\theta(b\theta-2)}}{\sqrt{bk^2(b\omega_1-a)}} + v_2 + v_4\right)\right) + A_{15} + 1\right)}. \tag{51}$$

After substituting Equation (51) into Equation (10), we obtain

$$\Delta_{2PCK}(\sigma) = \frac{\left(J_1 \exp\left(k\left(\frac{\sigma\sqrt{2\omega_1(b\theta-1)^2-2a\theta(b\theta-2)}}{\sqrt{bk^2(b\omega_1-a)}} + v_2 + v_4\right)\right) + A_{14} - 1\right)^2}{bc\left(J_1 \exp\left(k\left(\frac{\sigma\sqrt{2\omega_1(b\theta-1)^2-2a\theta(b\theta-2)}}{\sqrt{bk^2(b\omega_1-a)}} + v_2 + v_4\right)\right) + A_{15} + 1\right)^2}, \tag{52}$$

where

$$\begin{aligned} A_{14} = J_3\sqrt{a\theta(2-b\theta)+\omega_1(b\theta-1)^2}\exp\left(k\left(\frac{\sigma\sqrt{a\theta(2-b\theta)+\omega_1(b\theta-1)^2}}{\sqrt{2}\sqrt{bk^2\left(b\omega_1-a\right)}} + v_2\right)\right) \\ \cdot \sinh\left(k\left(\frac{\sigma\sqrt{a\theta(2-b\theta)+\omega_1(b\theta-1)^2}}{\sqrt{2}\sqrt{bk^2\left(b\omega_1-a\right)}} + v_8\right)\right) \end{aligned} \tag{53}$$

and

$$A_{15} = J_3\sqrt{bk^2\left(b\omega_1 - a\right)}\exp\left(k\left(\frac{\sigma\sqrt{a\theta(2-b\theta)+\omega_1(b\theta-1)^2}}{\sqrt{2}\sqrt{bk^2\left(b\omega_1-a\right)}}+v_2\right)\right) \cdot\cosh\left(k\left(\frac{\sigma\sqrt{a\theta(2-b\theta)+\omega_1(b\theta-1)^2}}{\sqrt{2}\sqrt{bk^2\left(b\omega_1-a\right)}}+v_8\right)\right). \tag{54}$$

Substituting Equations (51) and (52) into Equation (5) gives a PCK wave solution for Equation (1) as

$$G_{2PCK}(x,t) = \frac{ik\exp\left(\frac{i(\theta(2at-bx)+\omega_1(t-b\theta t))}{b}\right)\left(J_1\exp\left(k\left(\frac{(x-t\omega_1)\sqrt{2\omega_1(b\theta-1)^2-2a\theta(b\theta-2)}}{\sqrt{bk^2(b\omega_1-a)}}+v_2+v_4\right)\right)+A_{16}-1\right)}{\sqrt{2}\sqrt{c}\sqrt{d}\left(J_1\exp\left(k\left(\frac{(x-t\omega_1)\sqrt{2\omega_1(b\theta-1)^2-2a\theta(b\theta-2)}}{\sqrt{bk^2(b\omega_1-a)}}+v_2+v_4\right)\right)+A_{17}+1\right)}, \tag{55}$$

$$H_{2PCK}(x,t) = \frac{\left(J_1\exp\left(k\left(\frac{(x-t\omega_1)\sqrt{2\omega_1(b\theta-1)^2-2a\theta(b\theta-2)}}{\sqrt{bk^2(b\omega_1-a)}}+v_2+v_4\right)\right)+A_{16}-1\right)^2}{bc\left(J_1\exp\left(k\left(\frac{(x-t\omega_1)\sqrt{2\omega_1(b\theta-1)^2-2a\theta(b\theta-2)}}{\sqrt{bk^2(b\omega_1-a)}}+v_2+v_4\right)\right)+A_{17}+1\right)^2}, \tag{56}$$

where

$$A_{16} = J_3\exp\left(k\left(\frac{(x-t\omega_1)\sqrt{a\theta(2-b\theta)+\omega_1(b\theta-1)^2}}{\sqrt{2}\sqrt{bk^2\left(b\omega_1-a\right)}}+v_2\right)\right) \cdot\sinh\left(k\left(\frac{(x-t\omega_1)\sqrt{a\theta(2-b\theta)+\omega_1(b\theta-1)^2}}{\sqrt{2}\sqrt{bk^2\left(b\omega_1-a\right)}}+v_8\right)\right)\sqrt{a\theta(2-b\theta)+\omega_1(b\theta-1)^2} \tag{57}$$

and

$$A_{17} = J_3\exp\left(k\left(\frac{(x-t\omega_1)\sqrt{a\theta(2-b\theta)+\omega_1(b\theta-1)^2}}{\sqrt{2}\sqrt{bk^2\left(b\omega_1-a\right)}}+v_2\right)\right) \cdot\cosh\left(k\left(\frac{(x-t\omega_1)\sqrt{a\theta(2-b\theta)+\omega_1(b\theta-1)^2}}{\sqrt{2}\sqrt{bk^2\left(b\omega_1-a\right)}}+v_8\right)\right)\sqrt{bk^2\left(b\omega_1-a\right)}. \tag{58}$$

For illustration purposes, Figures 11, 12, 13 and 14 show some of these periodic cross kink waves. In particular, Figure 11 shows the solution $G_{1PCK}(x,t)$ corresponding to Equation (46) using the parameter values $v_2 = 0.4$, $v_4 = 0.8$, $v_6 = 2.3$, $J_1 = 9.1$, $J_2 = 5.9$, $J_4 = 1.2$, $a = 9.1$, $b = 5.0$, $c = 3.5$, $d = 1$, $k = 1.1$, $\omega_1 = 0.99$ and $\theta = 0.33$. The solution $H_{1PCK}(x,t)$ from Equation (47) is shown in Figure 12 for the same choice of parameter values. In turn, the solution $G_{2PCK}(x,t)$ from Equation (55) is shown in Figure 13 using $v_2 = 1.1$, $v_4 = 0.4$, $v_8 = 2.8$, $J_1 = 1.2$, $J_3 = 0.7$, $a = 0.2$, $b = 0.2$, $c = 1.9$, $d = 1$, $k = 0.8$, $\omega_1 = 0.1$ and $\theta = 2.9$. Meanwhile, the solution $H_{2PCK}(x,t)$ corresponding to Equation (56) is presented in Figure 14 for the same parameter set.

4.5. Homoclinic breather (HB)

This pattern of waves is reached by using (see [55])

$$\Phi(\sigma) = J_1\exp\left(k\left(\sigma v_3+v_4\right)\right)+\exp\left(-k\left(\sigma v_1+v_2\right)\right)+J_2\cos\left(k\left(\sigma v_5+v_6\right)\right). \tag{59}$$

By substituting Equation (59) and its first three derivatives into Equation (13), we obtained a simplified expression. We assemble similar terms together, and equate each expression's coefficients to zero. Thus, we obtained the following sets of constant values:

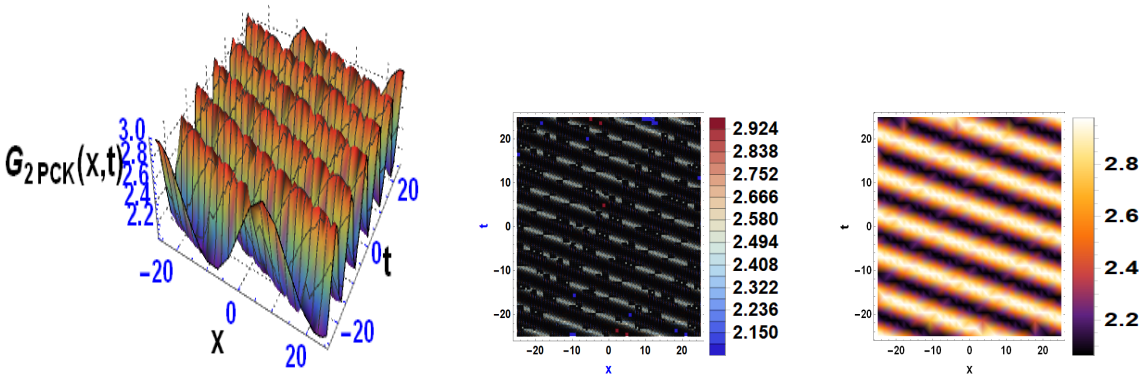

(a) (b) (c)

Figure 13: (a) Three-dimensional plot, (b) contour plot and (c) density plot corresponding to the function G_{2PCK} versus x and t. We used the parameters $v_2 = 1.1$, $v_4 = 0.4$, $v_8 = 2.8$, $J_1 = 1.2$, $J_3 = 0.7$, $a = 0.2$, $b = 0.2$, $c = 1.9$, $d = 1$, $k = 0.8$, $\omega_1 = 0.1$ and $\theta = 2.9$.

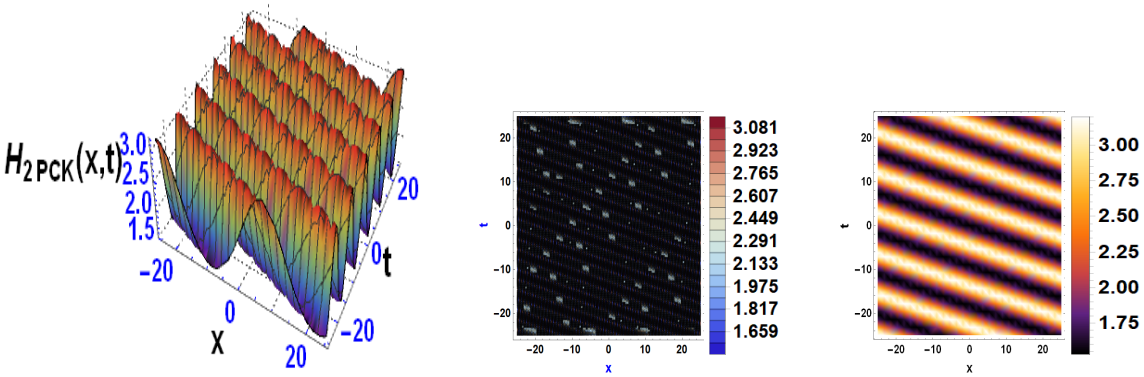

(a) (b) (c)

Figure 14: (a) Three-dimensional plot, (b) contour plot and (c) density plot corresponding to the function H_{2PCK} versus x and t. We used the parameters $v_2 = 1.1$, $v_4 = 0.4$, $v_8 = 2.8$, $J_1 = 1.2$, $J_3 = 0.7$, $a = 0.2$, $b = 0.2$, $c = 1.9$, $d = 1$, $k = 0.8$, $\omega_1 = 0.1$ and $\theta = 2.9$.

Family 1.

$$J_1 = 0,$$

$$v_1 = \frac{\sqrt{-ab\theta^2 + 2a\theta + b^2\theta^2\omega_1 - 2b\theta\omega_1 + \omega_1}}{\sqrt{2b^2k^2\omega_1 - 2abk^2}},$$

$$v_5 = -\frac{\sqrt{-ab\theta^2 + 2a\theta + b^2\theta^2\omega_1 - 2b\theta\omega_1 + \omega_1}}{\sqrt{2}\sqrt{abk^2 - b^2k^2\omega_1}},$$

$$R = \frac{i}{\sqrt{c}\sqrt{d}}.$$

Substituting them into Equation (59) and then the result into Equation (12), we reach

$$\Lambda_{1HB}(\sigma) = -\frac{ik\sqrt{a\theta(2-b\theta)+\omega_1(b\theta-1)^2}\left(\sqrt{bk^2\,(a-b\omega_1)} - A_{18}J_2\sqrt{bk^2\,(b\omega_1-a)}\right)}{\sqrt{2}\sqrt{c}\sqrt{d}\,(A_{19}J_2+1)\,\sqrt{-b^2k^4\,(a-b\omega_1)^2}}. \quad (60)$$

Substituting Equation (60) into Equation (10) gives

$$\Delta_{1HB}(\sigma) = \frac{\left(a\theta(b\theta-2)-\omega_1(b\theta-1)^2\right)\left(\sqrt{bk^2\,(a-b\omega_1)} - A_{18}J_2\sqrt{bk^2\,(b\omega_1-a)}\right)^2}{b^2ck^2\,(A_{19}J_2+1)^2\,(b\omega_1-a)}, \quad (61)$$

where

$$A_{18} = \exp\left(k\left(\frac{\sigma\sqrt{a\theta(2-b\theta)+\omega_1(b\theta-1)^2}}{\sqrt{2}\sqrt{bk^2\left(b\omega_1-a\right)}}+v_2\right)\right) \tag{62}$$

$$\cdot\sin\left(k\left(v_6-\frac{\sigma\sqrt{a\theta(2-b\theta)+\omega_1(b\theta-1)^2}}{\sqrt{2}\sqrt{bk^2\left(a-b\omega_1\right)}}\right)\right), \tag{63}$$

$$A_{19} = \exp\left(k\left(\frac{\sigma\sqrt{a\theta(2-b\theta)+\omega_1(b\theta-1)^2}}{\sqrt{2}\sqrt{bk^2\left(b\omega_1-a\right)}}+v_2\right)\right) \tag{64}$$

$$\cdot\cos\left(k\left(v_6-\frac{\sigma\sqrt{a\theta(2-b\theta)+\omega_1(b\theta-1)^2}}{\sqrt{2}\sqrt{bk^2\left(a-b\omega_1\right)}}\right)\right). \tag{65}$$

Using Equations (60) and (61) into Equation (5) gives a HB wave solution for Equation (1), namely,

$$G_{1HB}(x,t) = -\frac{iA_6k\sqrt{a\theta(2-b\theta)+\omega_1(b\theta-1)^2}\left(\sqrt{bk^2\left(a-b\omega_1\right)}-A_{20}J_2\sqrt{bk^2\left(b\omega_1-a\right)}\right)}{\sqrt{2}\sqrt{c}\sqrt{d}\left(A_{21}J_2+1\right)\sqrt{-b^2k^4\left(a-b\omega_1\right)^2}}, \tag{66}$$

$$H_{1HB}(x,t) = \frac{\left(a\theta(b\theta-2)-\omega_1(b\theta-1)^2\right)\left(\sqrt{bk^2\left(a-b\omega_1\right)}-A_{20}J_2\sqrt{bk^2\left(b\omega_1-a\right)}\right)^2}{b^2ck^2\left(A_{21}J_2+1\right)^2\left(b\omega_1-a\right)}, \tag{67}$$

where

$$\begin{aligned} A_{20} &= \exp\left(k\left(\frac{\left(x-t\omega_1\right)\sqrt{a\theta(2-b\theta)+\omega_1(b\theta-1)^2}}{\sqrt{2}\sqrt{bk^2\left(b\omega_1-a\right)}}+v_2\right)\right) \\ &\cdot\sin\left(k\left(\frac{\left(t\omega_1-x\right)\sqrt{a\theta(2-b\theta)+\omega_1(b\theta-1)^2}}{\sqrt{2}\sqrt{bk^2\left(a-b\omega_1\right)}}+v_6\right)\right), \end{aligned} \tag{68}$$

and

$$\begin{aligned} A_{21} &= \exp\left(k\left(\frac{\left(x-t\omega_1\right)\sqrt{a\theta(2-b\theta)+\omega_1(b\theta-1)^2}}{\sqrt{2}\sqrt{bk^2\left(b\omega_1-a\right)}}+v_2\right)\right) \\ &\cdot\cos\left(k\left(\frac{\left(t\omega_1-x\right)\sqrt{a\theta(2-b\theta)+\omega_1(b\theta-1)^2}}{\sqrt{2}\sqrt{bk^2\left(a-b\omega_1\right)}}+v_6\right)\right). \end{aligned} \tag{69}$$

Family 2.

$$\begin{aligned} v_1 &= \frac{\sqrt{-ab\theta^2+2a\theta+b^2\theta^2\omega_1-2b\theta\omega_1+\omega_1}}{\sqrt{2b^2k^2\omega_1-2abk^2}}, \\ v_3 &= \frac{\sqrt{-ab\theta^2+2a\theta+b^2\theta^2\omega_1-2b\theta\omega_1+\omega_1}}{\sqrt{2b^2k^2\omega_1-2abk^2}}, \\ v_5 &= -\frac{\sqrt{-ab\theta^2+2a\theta+b^2\theta^2\omega_1-2b\theta\omega_1+\omega_1}}{\sqrt{2}\sqrt{abk^2-b^2k^2\omega_1}}, \\ R &= -\frac{i}{\sqrt{c}\sqrt{d}}. \end{aligned}$$

Substituting these constants into Equation (59) and then the result into Equation (12), we have

$$\Lambda_{2HB}(\sigma) = -\frac{ik\sqrt{a\theta(2-b\theta)+\omega_1(b\theta-1)^2}\left(A_{22}J_2\sqrt{bk^2\left(b\omega_1-a\right)}\sin\left(k\left(v_6-\frac{\sigma\sqrt{a\theta(2-b\theta)+\omega_1(b\theta-1)^2}}{\sqrt{2}\sqrt{bk^2(a-b\omega_1)}}\right)\right)\right)}{\sqrt{2}\sqrt{c}\sqrt{d}\sqrt{-b^2k^4\left(a-b\omega_1\right)^2}\left(A_{23}J_2\cos\left(k\left(v_6-\frac{\sigma\sqrt{a\theta(2-b\theta)+\omega_1(b\theta-1)^2}}{\sqrt{2}\sqrt{bk^2(a-b\omega_1)}}\right)\right)+1\right)}. \tag{70}$$

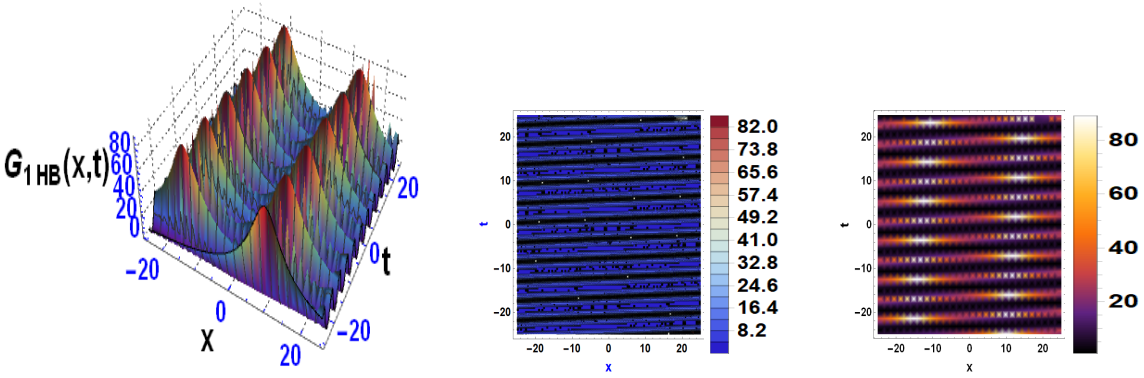

(a) (b) (c)

Figure 15: (a) Three-dimensional plot, (b) contour plot and (c) density plot corresponding to the function G_{1HB} versus x and t. We used the parameters $v_2 = 0.1$, $v_6 = 0.1$, $J_2 = 3.9$, $a = 9.8$, $b = 0.1$, $c = 0.7$, $d = 1$, $k = 6.9$, $\omega_1 = 0.1$ and $\theta = 9.4$.

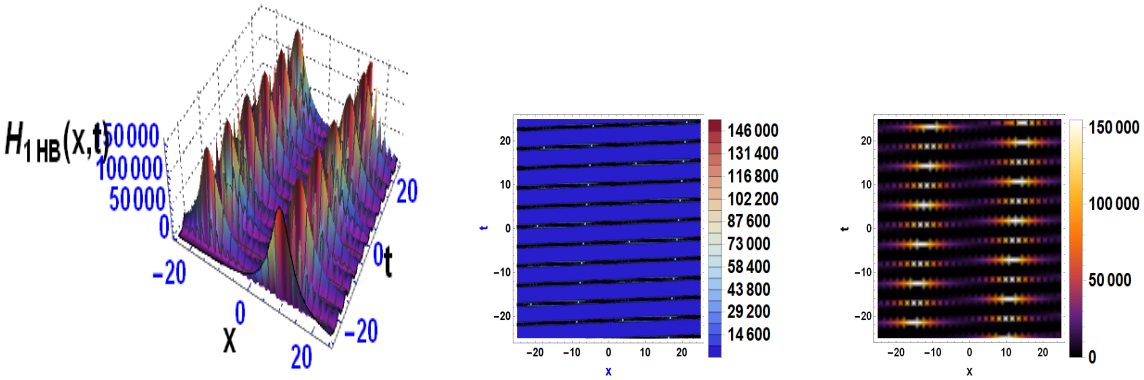

(a) (b) (c)

Figure 16: (a) Three-dimensional plot, (b) contour plot and (c) density plot corresponding to the function H_{1HB} versus x and t. We used the parameters $v_2 = 0.1$, $v_6 = 0.1$, $J_2 = 3.9$, $a = 9.8$, $b = 0.1$, $c = 0.7$, $d = 1$, $k = 6.9$, $\omega_1 = 0.1$ and $\theta = 9.4$.

Substituting Equation (70) into Equation (10) gives

$$\Delta_{2HB}(\sigma) = -\frac{\left(a\theta(2-b\theta)+\omega_1(b\theta-1)^2\right)\left(A_{22}J_2\sqrt{bk^2\left(b\omega_1-a\right)}\sin\left(k\left(v_6-\frac{\sigma\sqrt{a\theta(2-b\theta)+\omega_1(b\theta-1)^2}}{\sqrt{2}\sqrt{bk^2(a-b\omega_1)}}\right)\right)\right)^2}{b^2ck^2\left(b\omega_1-a\right)\left(A_{23}J_2\cos\left(k\left(v_6-\frac{\sigma\sqrt{a\theta(2-b\theta)+\omega_1(b\theta-1)^2}}{\sqrt{2}\sqrt{bk^2(a-b\omega_1)}}\right)\right)+1\right)^2}, \tag{71}$$

where

$$\begin{aligned} A_{22} = {} & J_1\sqrt{bk^2\left(a-b\omega_1\right)}\exp\left(k\left(\frac{\sigma\sqrt{2\omega_1(b\theta-1)^2-2a\theta(b\theta-2)}}{\sqrt{bk^2\left(b\omega_1-a\right)}}+v_2+v_4\right)\right) \\ & +\exp\left(k\left(\frac{\sigma\sqrt{a\theta(2-b\theta)+\omega_1(b\theta-1)^2}}{\sqrt{2}\sqrt{bk^2\left(b\omega_1-a\right)}}+v_2\right)\right)-\sqrt{bk^2\left(a-b\omega_1\right)} \end{aligned} \tag{72}$$

and

$$\begin{aligned} A_{23} = {} & J_1\exp\left(k\left(\frac{\sigma\sqrt{2\omega_1(b\theta-1)^2-2a\theta(b\theta-2)}}{\sqrt{bk^2\left(b\omega_1-a\right)}}+v_2+v_4\right)\right) \\ & +\exp\left(k\left(\frac{\sigma\sqrt{a\theta(2-b\theta)+\omega_1(b\theta-1)^2}}{\sqrt{2}\sqrt{bk^2\left(b\omega_1-a\right)}}+v_2\right)\right). \end{aligned} \tag{73}$$

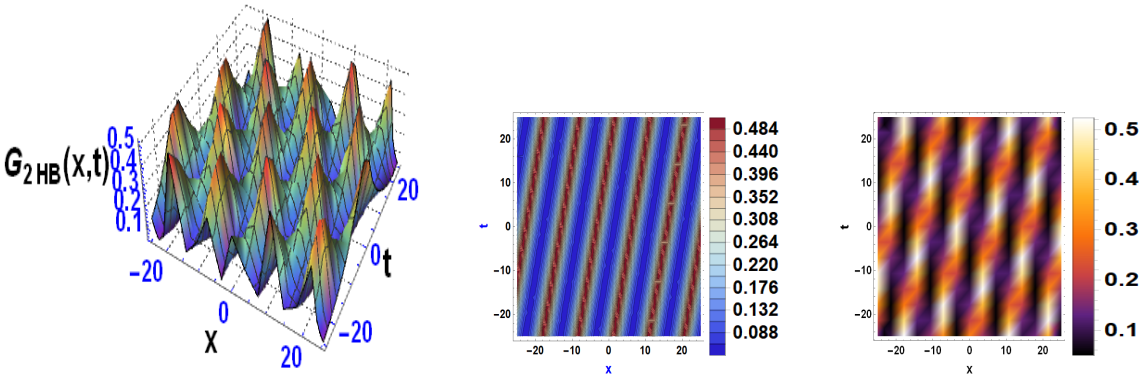

(a) (b) (c)

Figure 17: (a) Three-dimensional plot, (b) contour plot and (c) density plot corresponding to the function G_{2HB} versus x and t. We used the parameters $v_2 = 1.4$, $v_4 = 0.6$, $v_6 = 7.7$, $J_1 = 5.2$, $J_2 = 8.1$, $a = 1.5$, $b = 2.7$, $c = 4.1$, $d = 1$, $k = 0.1$, $\omega_1 = 0.2$ and $\theta = 0.4$.

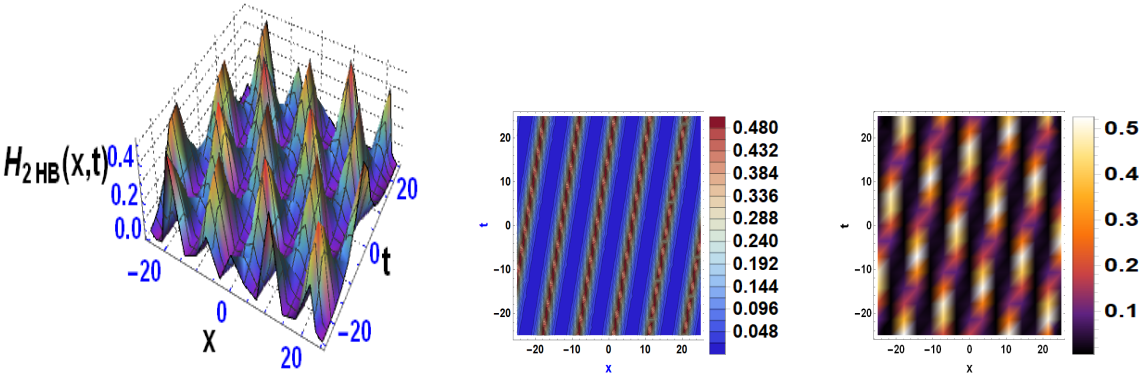

(a) (b) (c)

Figure 18: (a) Three-dimensional plot, (b) contour plot and (c) density plot corresponding to the function H_{2HB} versus x and t. We used the parameters $v_2 = 1.4$, $v_4 = 0.6$, $v_6 = 7.7$, $J_1 = 5.2$, $J_2 = 8.1$, $a = 1.5$, $b = 2.7$, $c = 4.1$, $d = 1$, $k = 0.1$, $\omega_1 = 0.2$ and $\theta = 0.4$.

Using Equations (70) and (71) into Equation (5) gives the HB wave solution for Equation (1):

$$G_{2HB}(x,t) = -\frac{ik\sqrt{a\theta(2-b\theta)+\omega_1(b\theta-1)^2}\exp\left(\frac{i(\theta(2at-bx)+\omega_1(t-b\theta t))}{b}\right)\left(A_{24}J_2\sqrt{bk^2(b\omega_1-a)}\sin\left(k\left(\frac{(t\omega_1-x)\sqrt{a\theta(2-b\theta)+\omega_1(b\theta-1)^2}}{\sqrt{2}\sqrt{bk^2(a-b\omega_1)}}+v_6\right)\right)\right)}{\sqrt{2}\sqrt{c}\sqrt{d}\sqrt{-b^2k^4(a-b\omega_1)^2}\left(A_{25}J_2\cos\left(k\left(\frac{(t\omega_1-x)\sqrt{a\theta(2-b\theta)+\omega_1(b\theta-1)^2}}{\sqrt{2}\sqrt{bk^2(a-b\omega_1)}}+v_6\right)\right)+1\right)} \tag{74}$$

$$H_{2HB}(x,t) = -\frac{\left(a\theta(2-b\theta)+\omega_1(b\theta-1)^2\right)\left(A_{24}J_2\sqrt{bk^2(b\omega_1-a)}\sin\left(k\left(\frac{(t\omega_1-x)\sqrt{a\theta(2-b\theta)+\omega_1(b\theta-1)^2}}{\sqrt{2}\sqrt{bk^2(a-b\omega_1)}}+v_6\right)\right)\right)^2}{b^2ck^2(b\omega_1-a)\left(A_{25}J_2\cos\left(k\left(\frac{(t\omega_1-x)\sqrt{a\theta(2-b\theta)+\omega_1(b\theta-1)^2}}{\sqrt{2}\sqrt{bk^2(a-b\omega_1)}}+v_6\right)\right)+1\right)^2}, \tag{75}$$

where

$$\begin{aligned} A_{24} = {} & J_1\sqrt{bk^2\left(a-b\omega_1\right)}\exp\left(k\left(\frac{\left(x-t\omega_1\right)\sqrt{2\omega_1(b\theta-1)^2-2a\theta(b\theta-2)}}{\sqrt{bk^2\left(b\omega_1-a\right)}}+v_2+v_4\right)\right) \\ & +\exp\left(k\left(\frac{\left(x-t\omega_1\right)\sqrt{a\theta(2-b\theta)+\omega_1(b\theta-1)^2}}{\sqrt{2}\sqrt{bk^2\left(b\omega_1-a\right)}}+v_2\right)\right)-\sqrt{bk^2\left(a-b\omega_1\right)} \end{aligned} \tag{76}$$

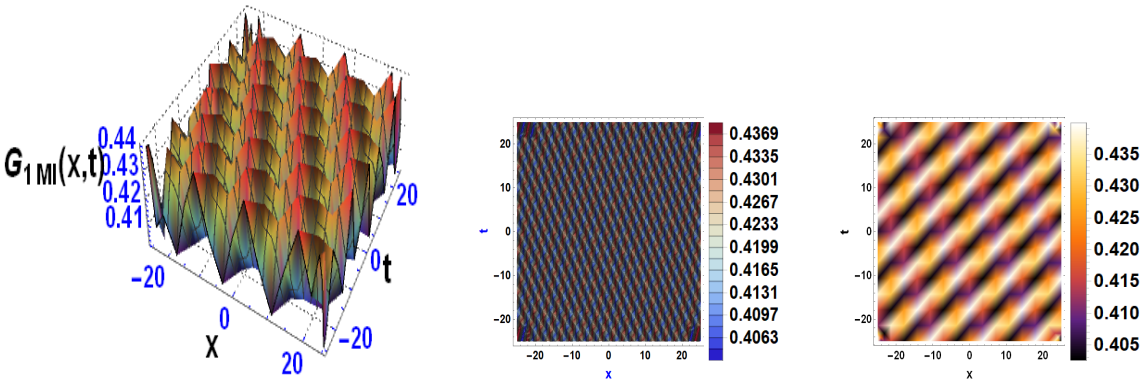

(a) (b) (c)

Figure 19: (a) Three-dimensional plot, (b) contour plot and (c) density plot corresponding to the function G_{1MI} versus x and t. We used the parameters $v_2 = 0.4$, $v_4 = 2.4$, $v_6 = 0.5$, $J_1 = 1.6$, $J_3 = 5.9$, $J_4 = 1.2$, $a = 0.5$, $b = 1.2$, $c = 6.8$, $d = 1$, $k = 9.4$, $\omega_1 = 0.3$ and $\theta = 1.1$.

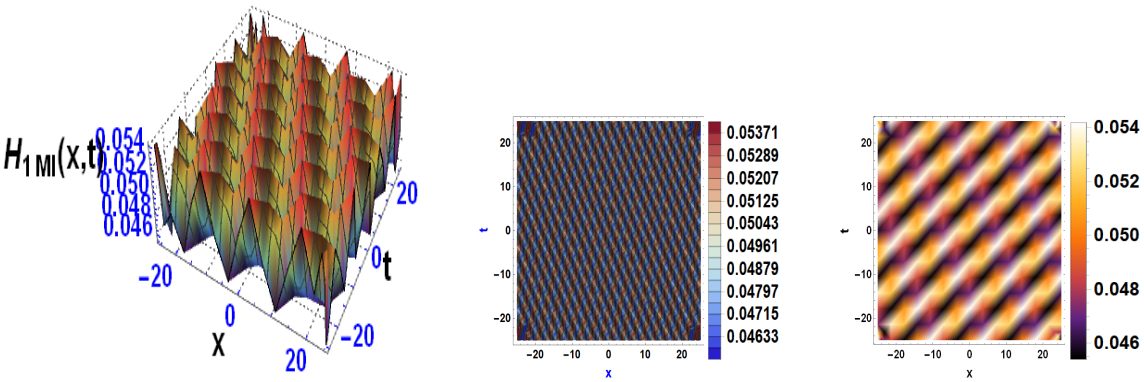

(a) (b) (c)

Figure 20: (a) Three-dimensional plot, (b) contour plot and (c) density plot corresponding to the function H_{1MI} versus x and t. We used the parameters $v_2 = 0.4$, $v_4 = 2.4$, $v_6 = 0.5$, $J_1 = 1.6$, $J_3 = 5.9$, $J_4 = 1.2$, $a = 0.5$, $b = 1.2$, $c = 6.8$, $d = 1$, $k = 9.4$, $\omega_1 = 0.3$ and $\theta = 1.1$.

and

$$A_{25} = J_1 \exp\left(k\left(\frac{(x - t\omega_1)\sqrt{2\omega_1(b\theta-1)^2 - 2a\theta(b\theta-2)}}{\sqrt{bk^2(b\omega_1 - a)}} + v_2 + v_4\right)\right) + \exp\left(k\left(\frac{(x - t\omega_1)\sqrt{a\theta(2-b\theta) + \omega_1(b\theta-1)^2}}{\sqrt{2}\sqrt{bk^2(b\omega_1 - a)}} + v_2\right)\right). \tag{77}$$

Figures 15 and 16 portray periodic homoclinic breather wave, while Figures 17 and 18 show multiple homoclinic breather waves. In particular, Figure 15 depicts the solution $G_{1HB}(x,t)$ corresponding to Equation (66) for the parameter values $v_2 = 0.1$, $v_6 = 0.1$, $J_2 = 3.9$, $a = 9.8$, $b = 0.1$, $c = 0.7$, $d = 1$, $k = 6.9$, $\omega_1 = 0.1$ and $\theta = 9.4$. Figure 16 shows the solution $H_{1HB}(x,t)$ obtained from Equation (67) for the same choice of parameters as in Figure 15. In turn, Figure 17 shows the solution $G_{2HB}(x,t)$ from Equation (74) for the parameter values $v_2 = 1.4$, $v_4 = 0.6$, $v_6 = 7.7$, $J_1 = 5.2$, $J_2 = 8.1$, $a = 1.5$, $b = 2.7$, $c = 4.1$, $d = 1$, $k = 0.1$, $\omega_1 = 0.2$ and $\theta = 0.4$. Figure (18)) is the solution $H_{2HB}(x,t)$ corresponding to Equation (75) for the same choice of parameter values as Figure 17.

4.6. Mixed waves (MI)

This pattern of waves is derived by using (see [55])

$$\begin{aligned}\Phi(\sigma) = J_1 \exp\left(k\left(\sigma v_1 + v_2\right)\right) + J_2 \exp\left(-k\left(\sigma v_1 + v_2\right)\right) \\ + J_3 \sin\left(k\left(\sigma v_3 + v_4\right)\right) + J_4 \sinh\left(k\left(\sigma v_5 + v_6\right)\right).\end{aligned} \tag{78}$$

By substituting Equation (78) and its first three derivatives into Equation (13), and proceeding as in the previous sections, we obtain the following sets of constant values:

Family 1.

$$\begin{aligned} J_2 &= 0, \\ v_1 &= \frac{\sqrt{-ab\theta^2 + 2a\theta + b^2\theta^2\omega_1 - 2b\theta\omega_1 + \omega_1}}{\sqrt{2b^2k^2\omega_1 - 2abk^2}}, \\ v_3 &= -\frac{\sqrt{-ab\theta^2 + 2a\theta + b^2\theta^2\omega_1 - 2b\theta\omega_1 + \omega_1}}{\sqrt{2}\sqrt{abk^2 - b^2k^2\omega_1}}, \\ v_5 &= \frac{\sqrt{-ab\theta^2 + 2a\theta + b^2\theta^2\omega_1 - 2b\theta\omega_1 + \omega_1}}{\sqrt{2b^2k^2\omega_1 - 2abk^2}}, \\ R &= \frac{i}{\sqrt{c}\sqrt{d}}. \end{aligned}$$

Substituting them into Equation (78) and then the outcome into Equation (12), we obtain

$$\Lambda_{1MI}(\sigma) = \frac{ik\sqrt{a\theta(2-b\theta)+\omega_1(b\theta-1)^2}\left(A_{26}\sqrt{bk^2(a-b\omega_1)} - J_3\sqrt{bk^2(b\omega_1-a)}\cos\left(k\left(v_4 - \frac{\sigma\sqrt{a\theta(2-b\theta)+\omega_1(b\theta-1)^2}}{\sqrt{2}\sqrt{bk^2(a-b\omega_1)}}\right)\right)\right)}{\sqrt{2}\sqrt{c}\sqrt{d}\sqrt{-b^2k^4(a-b\omega_1)^2}\left(J_4\sinh\left(k\left(\frac{\sigma\sqrt{a\theta(2-b\theta)+\omega_1(b\theta-1)^2}}{\sqrt{2}\sqrt{bk^2(b\omega_1-a)}} + v_6\right)\right) + A_{27}\right)}. \tag{79}$$

Putting Equation (79) into Equation (10) gives

$$\Delta_{1MI}(\sigma) = -\frac{\left(a\theta(2-b\theta)+\omega_1(b\theta-1)^2\right)\left(A_{26}\sqrt{bk^2(a-b\omega_1)} - J_3\sqrt{bk^2(b\omega_1-a)}\cos\left(k\left(v_4 - \frac{\sigma\sqrt{a\theta(2-b\theta)+\omega_1(b\theta-1)^2}}{\sqrt{2}\sqrt{bk^2(a-b\omega_1)}}\right)\right)\right)^2}{b^2ck^2(b\omega_1-a)\left(J_4\sinh\left(k\left(\frac{\sigma\sqrt{a\theta(2-b\theta)+\omega_1(b\theta-1)^2}}{\sqrt{2}\sqrt{bk^2(b\omega_1-a)}} + v_6\right)\right) + A_{27}\right)^2}, \tag{80}$$

where

$$\begin{aligned} A_{26} = J_1 \exp\left(k\left(\frac{\sigma\sqrt{a\theta(2-b\theta)+\omega_1(b\theta-1)^2}}{\sqrt{2}\sqrt{bk^2\left(b\omega_1-a\right)}} + v_2\right)\right) \\ + J_4 \cosh\left(k\left(\frac{\sigma\sqrt{a\theta(2-b\theta)+\omega_1(b\theta-1)^2}}{\sqrt{2}\sqrt{bk^2\left(b\omega_1-a\right)}} + v_6\right)\right), \end{aligned} \tag{81}$$

$$\begin{aligned} A_{27} = J_1 \exp\left(k\left(\frac{\sigma\sqrt{a\theta(2-b\theta)+\omega_1(b\theta-1)^2}}{\sqrt{2}\sqrt{bk^2\left(b\omega_1-a\right)}} + v_2\right)\right) \\ + J_3 \sin\left(k\left(v_4 - \frac{\sigma\sqrt{a\theta(2-b\theta)+\omega_1(b\theta-1)^2}}{\sqrt{2}\sqrt{bk^2\left(a-b\omega_1\right)}}\right)\right). \end{aligned} \tag{82}$$

Applying Equations (79) and (80) in Equation (5) gives the required MI wave solutions for Equation (1) as

$$G_{1MI}(x,t) = \frac{iA_6k\sqrt{a\theta(2-b\theta)+\omega_1(b\theta-1)^2}\left(A_{28}\sqrt{bk^2(a-b\omega_1)} - J_3\sqrt{bk^2(b\omega_1-a)}\cos\left(k\left(\frac{(t\omega_1-x)\sqrt{a\theta(2-b\theta)+\omega_1(b\theta-1)^2}}{\sqrt{2}\sqrt{bk^2(a-b\omega_1)}} + v_4\right)\right)\right)}{\sqrt{2}\sqrt{c}\sqrt{d}\sqrt{-b^2k^4(a-b\omega_1)^2}\left(J_4\sinh\left(k\left(\frac{(x-t\omega_1)\sqrt{a\theta(2-b\theta)+\omega_1(b\theta-1)^2}}{\sqrt{2}\sqrt{bk^2(b\omega_1-a)}} + v_6\right)\right) + A_{29}\right)}, \tag{83}$$

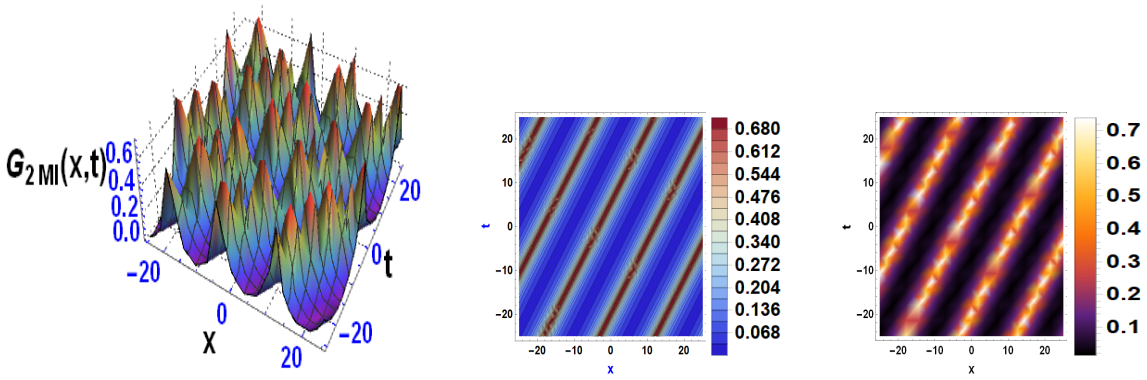

(a) (b) (c)

Figure 21: (a) Three-dimensional plot, (b) contour plot and (c) density plot corresponding to the function G_{2MI} versus x and t. We used the parameters $v_4 = 0.5$, $v_6 = 0.5$, $J_3 = 5.9$, $J_4 = 1.2$, $a = 5.7$, $b = 7.6$, $c = 4.0$, $d = 1$, $k = 1.2$, $\omega_1 = 0.6$ and $\theta = 0.1$.

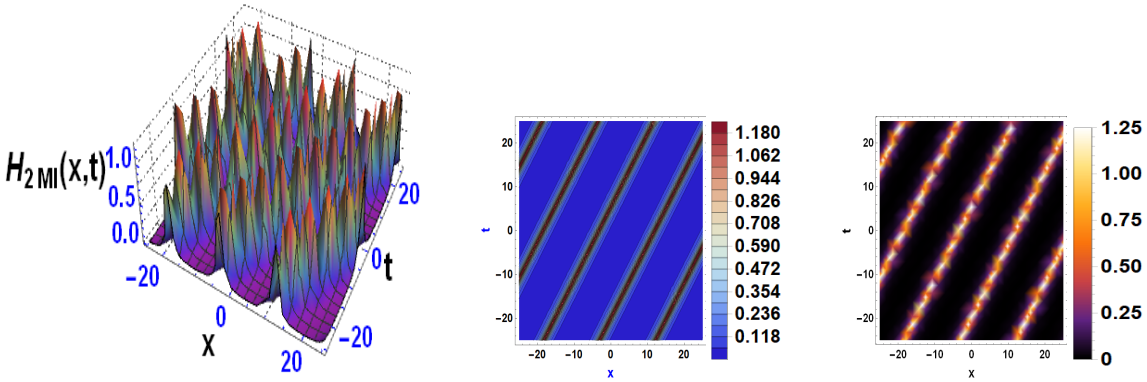

(a) (b) (c)

Figure 22: (a) Three-dimensional plot, (b) contour plot and (c) density plot corresponding to the function H_{2MI} versus x and t. We used the parameters $v_4 = 0.5$, $v_6 = 0.5$, $J_3 = 5.9$, $J_4 = 1.2$, $a = 5.7$, $b = 7.6$, $c = 4.0$, $d = 1$, $k = 1.2$, $\omega_1 = 0.6$ and $\theta = 0.1$.

$$H_{1MI}(x,t) = -\frac{(a\theta(2-b\theta)+\omega_1(b\theta-1)^2)\left(A_{28}\sqrt{bk^2(a-b\omega_1)}-J_3\sqrt{bk^2(b\omega_1-a)}\cos\left(k\left(\frac{(t\omega_1-x)\sqrt{a\theta(2-b\theta)+\omega_1(b\theta-1)^2}}{\sqrt{2}\sqrt{bk^2(a-b\omega_1)}}+v_4\right)\right)\right)^2}{b^2ck^2(b\omega_1-a)\left(J_4\sinh\left(k\left(\frac{(x-t\omega_1)\sqrt{a\theta(2-b\theta)+\omega_1(b\theta-1)^2}}{\sqrt{2}\sqrt{bk^2(b\omega_1-a)}}+v_6\right)\right)+A_{29}\right)^2}, \tag{84}$$

where

$$\begin{aligned} A_{28} = {} & J_1 \exp\left(k\left(\frac{(x-t\omega_1)\sqrt{a\theta(2-b\theta)+\omega_1(b\theta-1)^2}}{\sqrt{2}\sqrt{bk^2\left(b\omega_1-a\right)}}+v_2\right)\right) \\ & + J_4\cosh\left(k\left(\frac{(x-t\omega_1)\sqrt{a\theta(2-b\theta)+\omega_1(b\theta-1)^2}}{\sqrt{2}\sqrt{bk^2\left(b\omega_1-a\right)}}+v_6\right)\right) \end{aligned} \tag{85}$$

and

$$\begin{aligned} A_{29} = {} & J_1 \exp\left(k\left(\frac{(x-t\omega_1)\sqrt{a\theta(2-b\theta)+\omega_1(b\theta-1)^2}}{\sqrt{2}\sqrt{bk^2\left(b\omega_1-a\right)}}+v_2\right)\right) \\ & + J_3\sin\left(k\left(\frac{(t\omega_1-x)\sqrt{a\theta(2-b\theta)+\omega_1(b\theta-1)^2}}{\sqrt{2}\sqrt{bk^2\left(a-b\omega_1\right)}}+v_4\right)\right). \end{aligned} \tag{86}$$

Family 2.

$$v_3 = \frac{\sqrt{-ab\theta^2 + 2a\theta + b^2\theta^2\omega_1 - 2b\theta\omega_1 + \omega_1}}{\sqrt{2}\sqrt{abk^2 - b^2k^2\omega_1}},$$

$$v_5 = \frac{\sqrt{-ab\theta^2 + 2a\theta + b^2\theta^2\omega_1 - 2b\theta\omega_1 + \omega_1}}{\sqrt{2b^2k^2\omega_1 - 2abk^2}},$$

$$J_1 = 0,$$

$$J_2 = 0,$$

$$R = -\frac{i}{\sqrt{c}\sqrt{d}}.$$

Substituting these constants into Equation (78) and then the result into Equation (12), we have

$$\Lambda_{2MI}(\sigma) = -\frac{ik\sqrt{a\theta(2-b\theta)+\omega_1(b\theta-1)^2}\left(A_{30}J_3\sqrt{bk^2\left(b\omega_1-a\right)}\right)}{\sqrt{2}\sqrt{c}\sqrt{d}\left(J_3\sin\left(k\left(\frac{\sigma\sqrt{a\theta(2-b\theta)+\omega_1(b\theta-1)^2}}{\sqrt{2}\sqrt{bk^2(a-b\omega_1)}}+v_4\right)\right)+A_{31}\right)}. \tag{87}$$

Substituting Equation (87) into Equation (10) yields

$$\Delta_{2MI}(\sigma) = \frac{\left(a\theta(b\theta-2)-\omega_1(b\theta-1)^2\right)\left(A_{30}J_3\sqrt{bk^2\left(b\omega_1-a\right)}\right)^2}{bc\left(J_3\sin\left(k\left(\frac{\sigma\sqrt{a\theta(2-b\theta)+\omega_1(b\theta-1)^2}}{\sqrt{2}\sqrt{bk^2(a-b\omega_1)}}+v_4\right)\right)+A_{31}\right)^2}, \tag{88}$$

where

$$\begin{aligned} A_{30} = {} & J_4\sqrt{bk^2\left(a-b\omega_1\right)}\cosh\left(k\left(\frac{\sigma\sqrt{a\theta(2-b\theta)+\omega_1(b\theta-1)^2}}{\sqrt{2}\sqrt{bk^2\left(b\omega_1-a\right)}}+v_6\right)\right) \\ & +\cos\left(k\left(\frac{\sigma\sqrt{a\theta(2-b\theta)+\omega_1(b\theta-1)^2}}{\sqrt{2}\sqrt{bk^2\left(a-b\omega_1\right)}}+v_4\right)\right), \end{aligned} \tag{89}$$

and

$$A_{31} = J_4\sqrt{-b^2k^4\left(a-b\omega_1\right)^2}\sinh\left(k\left(\frac{\sigma\sqrt{a\theta(2-b\theta)+\omega_1(b\theta-1)^2}}{\sqrt{2}\sqrt{bk^2\left(b\omega_1-a\right)}}+v_6\right)\right). \tag{90}$$

Substituting Equations (87) and (88) into Equation (5) gives the MI wave solution for Equation (1):

$$G_{2MI}(x,t) = -\frac{iA_6k\sqrt{a\theta(2-b\theta)+\omega_1(b\theta-1)^2}\left(A_{32}J_3\sqrt{bk^2\left(b\omega_1-a\right)}\right)}{\sqrt{2}\sqrt{c}\sqrt{d}\left(J_3\sin\left(k\left(\frac{(x-t\omega_1)\sqrt{a\theta(2-b\theta)+\omega_1(b\theta-1)^2}}{\sqrt{2}\sqrt{bk^2(a-b\omega_1)}}+v_4\right)\right)+A_{33}\right)}, \tag{91}$$

$$H_{2MI}(x,t) = \frac{\left(a\theta(b\theta-2)-\omega_1(b\theta-1)^2\right)\left(A_{32}J_3\sqrt{bk^2\left(b\omega_1-a\right)}\right)^2}{bc\left(J_3\sin\left(k\left(\frac{(x-t\omega_1)\sqrt{a\theta(2-b\theta)+\omega_1(b\theta-1)^2}}{\sqrt{2}\sqrt{bk^2(a-b\omega_1)}}+v_4\right)\right)+A_{33}\right)^2}, \tag{92}$$

where

$$\begin{aligned} A_{32} = {} & J_4\sqrt{bk^2\left(a-b\omega_1\right)}\cosh\left(k\left(\frac{(x-t\omega_1)\sqrt{a\theta(2-b\theta)+\omega_1(b\theta-1)^2}}{\sqrt{2}\sqrt{bk^2\left(b\omega_1-a\right)}}+v_6\right)\right) \\ & +\cos\left(k\left(\frac{(x-t\omega_1)\sqrt{a\theta(2-b\theta)+\omega_1(b\theta-1)^2}}{\sqrt{2}\sqrt{bk^2\left(a-b\omega_1\right)}}+v_4\right)\right) \end{aligned} \tag{93}$$

and

$$A_{33} = J_4\sqrt{-b^2k^4\left(a-b\omega_1\right)^2}\sinh\left(k\left(\frac{\left(x-t\omega_1\right)\sqrt{a\theta(2-b\theta)+\omega_1(b\theta-1)^2}}{\sqrt{2}\sqrt{bk^2\left(b\omega_1-a\right)}}+v_6\right)\right). \quad (94)$$

In Figures 19, 20, 21 and (22, we provide graphs of mixtures of wave forms. The solution $G_{1MI}(x,t)$ corresponding to Equation (83) is shown in Figure 19 for the parameter values $v_2 = 0.4$, $v_4 = 2.4$, $v_6 = 0.5$, $J_1 = 1.6$, $J_3 = 5.9$, $J_4 = 1.2$, $a = 0.5$, $b = 1.2$, $c = 6.8$, $d = 1$, $k = 9.4$, $\omega_1 = 0.3$ and $\theta = 1.1$. Figure 20 is the solution $H_{1MI}(x,t)$ corresponding to Equation (84) with the same chosen parameter values as Figure 19. In turn, the solution $G_{2MI}(x,t)$ corresponding to Equation (91) is shown in Figure 21 for the parameter values $v_4 = 0.5$, $v_6 = 0.5$, $J_3 = 5.9$, $J_4 = 1.2$, $a = 5.7$, $b = 7.6$, $c = 4.0$, $d = 1$, $k = 1.2$, $\omega_1 = 0.6$ and $\theta = 0.1$. Figure 22 is obtained from Equation (84).

5. Discussion

This section displays the graphical representation of the travelling wave solutions found for the Heisenberg ferromagnet type of Akbota equation arising in surface geometry. The graphs, which were produced with mathematica, provides a clear representation of the soliton solutions found in the preceding section. Owing to the impact of graphical morphology on the traveling wave solutions' dynamics, we have illustrated a range of soliton solution types in three-dimensional and their corresponding contour and density plots, including M-shaped wave with rogue and kink shaped, multi wave solutions, periodic lump solution, periodic cross kink wave solution, homoclinic breather wave solution and mixed wave solution.

Figures (3) and (4) are acquired from the MRK wave function. Figures (3)(a) and (4) (a) show a 3D surface plot, which exhibits a periodic wave structure in space and time, reflecting traveling wave or soliton-like behavior.The crests and troughs represent regions of maximum and minimum amplitude, demonstrating the way that the wave continuously varies shape but preserves its ordered form. Figures (3) (b) and (4) (b) depict a contour plot, presenting the bird's eye view of the wave pattern focusing on periodicity and phase shift. Parallel nature of the contours indicates uniform propagation with unvarying velocity and wavelength typical of nonlinear wave propagation. On the other hand, Figures (3) (c) and (13) (c) illustrate a density plot, whose color saturation variation tells us about different amplitudes. Alternating high and low value bands establish periodic motion of the wave, and the smooth transition shows continuous and differentiable motion necessary in surface geometry and curve analysis.

Figures (5)(a) and (6)(a) arises from the MU wave function. A detailed wave interactions are given in Figure (6) (a), showing a very organized, multi-peaked wave profile with a checkerboard-type modulation, characteristic of nonlinear interactions or potential breather-type structures. In contrast to pure sinusoidal waves, the modulated nature of this structure indicates higher-order soliton interaction, quasi-periodicity, or interference effects. The associated contour plot in Figure (6) (b) shows a close-packed pattern of alternating wave crests and troughs, consisting of diagonal wavefronts reminiscent of a nontrivial dispersion relation.This periodicity in an ordered fashion can be indicative of wave turbulence, breather dynamics, or multi-soliton interactions. The intensity variation is also highlighted in the density plot in Figure (6) (c), where high-contrast regions indicate large wave amplitude modulations. The diagonal nature of these patterns supports complex wave dynamics, indicating multi wave shaped structures in certain cross-sectional profiles. Figures 4-6 extend this investigation to show extremely structured, multi-peak wave forms with closely packed, modulated patterns. In Figure (7) (a), the occurrence of sharp peaks and troughs indicates strongly nonlinear interactions, possibly of higher-order soliton structures or breather-type dynamics. The contour plot shown in Figure (7) (b) is a diagonal wavefront structure with well-behaved periodicity, establishing the interaction of dispersion and nonlinearity in determining wave propagation. Likewise, Figure (7) (c)

density plot verifies the existence of structured periodicity as well as modulation effects, enhancing the likelihood of breather-type dynamics. Figures (8) and (9) also obtained from MU wave function, have similar properties, with 3D surface plots in Figures (8) (a) and (9) (a) displaying complex wave structures characterized by sharp oscillations and multi-scale variations. Their respective contour and density plots indicate tilted alternating bands of peaks and troughs of waves and thus strong spatial periodicity coupled with modulated intensity variations. These observations indicate the occurrence of modulation instability effects, hybrid soliton-breather formations.

Figures (9) and (10) are acquired from the PL wave unction. Figures (9) (a) and (10) (a) illustrate features of periodic lump waves. A lump wave is a localized rational solution of some nonlinear wave equations, commonly an isolated peak in space and time. But periodic lump structures occur when such solutions recur periodically at regular intervals. In Figure 7(a), the 3D plot shows well-separated, localized peaks on a flat background, characteristic of periodic lump waves and not isolated solitons. The corresponding contour and density plots support this classification by showing localized high-intensity spots along a diagonal path, establishing the spatial and temporal periodicity of these structures. The same trend is seen in Figure 8, where a train of sharp, local peaks aligned in a periodic fashion further indicates the assignment to a periodic lump wave. Figures (11) to (14) represent PCK waves function, which are structured, traveling waves with periodically alternating space and time. The 3D plots in Figures (11) (a) and (12) (a) show periodic ridges similar to layered kinks that build a checkerboard-like periodic pattern. This implies the interactions of several kink-like waves moving periodically.The contour plots in Figures (11) (b) and (12) (b) show diagonal wavefronts characteristic of a propagating kink-like structure, smooth and periodic amplitude transitions characteristic of cross-kink interactions. The density plots in Figures (11) (c) and (12) (c) is also in line with this interpretation, showing alternating intensity bands with sharp transitions characteristic of periodic wave interactions.Consistent periodic cross-kink topologies are also noted in Figures (13) (a) and (14) (a), which each progressively illustrate more intricate periodic interactions indicating multiple frequency component wave formations or soliton modulation interaction. The contour Plots in Figures (13) (b) and (14) (b) have diagonal bands and intersecting wave patterns indicating cross-kink interactions. The appearance of non-uniform intensity variation signifies interactions of more than one periodic component. The density Plots in Figures (13) (c) and (14) (c) have alternating diagonal intensity bands affirm periodic kinks interacting in opposite directions. This again validates the cross-kink periodic structure, where the wave has repeating kink-like structures modulated by periodic oscillations.

The HB waves structures are defined by Figures (15) through (18), representing localized oscillating structures that return to the identical asymptotic state with increasing time tending to infinity. These are homoclinic orbits in dynamical systems and are generally discovered in integrable equations such as the nonlinear Schrödinger equation or sine-Gordon equation. The 3D plot in Figure (15) (a) indicates a localized oscillatory structure with periodic oscillations, which shows the presence of a homoclinic breather. The respective contour plot in Figure (15) (b) and density plot in Figure (15) (c) also support this classification through periodic energy localization and striped, repetitive patterns typical of breather solutions. Such features are seen in Figures (16) to (18), too, where oscillatory patterns, periodic modulations, and amplitude changes indicate the existence of homoclinic breather solutions in various parameter regimes. Figures (19) to (22) obtained from the MI wave function show unique nonlinear wave dynamics each with significant physical phenomena like modulation instability, breather wave formations, mixed wave interactions, and localization of energy. These data show the behavior of nonlinear waves for various conditions of parameters and reflect their role in areas including optical fiber communication, plasma physics, and theory of hydrodynamic waves. Figures (19) and (20) display a typical periodic modulation instability wave pattern. The periodicity in time and space can be visually inspected from the 3D plot in Figures (19) (a) and (20) (a),

showing exponential amplification of initial perturbations owing to nonlinearities. The contour plot in Figures (19) (b) and (10) (b) also display an apparent periodic modulation of wave amplitude, while the density plot in Figures (19) (c) and (10)1 (c) depict alternate high-energy and low-energy regions. This process shows that MI is the origin of energy localization, a major mechanism in the formation of rogue waves and soliton trains observed in nonlinear optics and ocean wave physics. The development of periodicity from homogeneous wave propagation is the beginning of instability-driven periodicity. Figures (21) and (22) demonstrate a high-order breather profile, which may be a precursor to the creation of rogue waves. The 3D plots in Figures (21) (a) and (22) (a) exhibit highly nonlinear behavior with steep crests and large changes in amplitude, consistent with the formation of rogue waves. The contour plots in Figures (21) (b) and (22) (b) demonstrate distinct bands of waves separated by areas of high energy, which confirm the presence of high-order breathers. The density plots in Figures (21) (c) and (22) (c) indicates high energy localization, typical in rogue wave precursors. These localized high-amplitude structures form as a result of nonlinear focusing effects, rendering them central to the comprehension of extreme wave events in plasma physics, fiber optics, and oceanography. The abrupt energy concentration proposes the possibility of the creation of rogue waves where nonlinear amplification causes unusual but immensely strong wave structures.

In total, the visual depictions obtained in these figures showcase a variety of wave phenomena ranging from soliton-like behavior and breather dynamics to periodic lump waves and periodic cross-kink structures. The dynamics of nonlinearity, dispersion, and modulation effects rule the evolution and stability of these waves, demonstrating the complicated character of wave interactions within nonlinear systems. These results deepen the knowledge on wave dynamics in mathematical physics and nonlinear wave theory.

6. Conclusion

In this paper, we have studied the Heisenberg ferromagnet type of Akbota problem arising in surface geometry for interaction between lump and periodic waves, periodic and cross kink wave, multi wave, homoclinic breather waves, mixed waves and interaction between M-shaped with rogue and kink waves. Under the impact of kinks and rogue waves, the M-shaped wave displays a profile with fluctuating peaks and troughs that can get more intricate and erratic. Complex wave behaviour results from these interactions, which induce large deformations in the wave's height and shape. Multiple wave trains or patterns existing simultaneously in different media, such sound, water, or electromagnetic fields, are referred to as multi waves. Either constructive or destructive interference can be used to increase or decrease the other overlapping waves. Beat frequencies and other complex patterns and behaviours are produced when several wave types, such as sinusoidal and rogue waves, combine to form mixed waves. When kinks in wave profiles interact with waves that occur regularly, they can cause disturbances that are localised and result in periodic cross-kink waves. Periodic lumps are stabilised in a moving frame but may move if system circumstances change. They are defined by recurrent "bumps" or peaks in space. Often unstable and exhibiting intricate interactions with their surroundings, homoclinic breathers can exhibit oscillations and localised patterns that result in breather splitting or fusing. By using ansatz transformations and Hirota bilinear approach, we were able to acquired solutions for all these wave structures and illustrate them in three dimensional, contour and density plots. All in all, this work advances the theoretical understanding of wave dynamics by employing the mathematical method of the Hirota bilinear technique and offers specific interpretations and applications in a number of scientific fields. From the prediction of catastrophic wave occurrences to the optimisation of wave-based technology, our findings have implications for a broad spectrum of physical phenomena and economic implications.

This study leaves a few doors open for future research. Generalizing the Hirota bilinear method to higher-dimensional models and other nonlinear systems may give further insights into wave phenomena of complex nature. Stability and dynamics of the obtained solutions, including experimental testing, would fill the gap between theory and practice. Numerical solutions

and analysis of wave interaction could introduce new hybrid structures and their possibility of application. Exploring the fractional and stochastic character of the Akbota equation would add more potential for its use. Studying the fractional form of the equation, where derivatives are replaced with fractional-order operators, could indicate new wave patterns and dynamics, for instance, solitons or breathers, particularly usable in memory effects or anomalous diffusion systems. Introduction of stochastic terms will allow wave behavior under conditions of random noise or fluctuations to be studied and result in more realistic models for real systems. Hybrids of fractional and stochastic approaches can be constructed and may provide better applicable models for sophisticated systems, including turbulent fluids, disordered materials, or membranes in biology. Last but not least, transferring these solutions to emerging technological areas, including optical communications, magnetic systems, and wave propagation under noise drive, may lead to enhanced performance and innovation in these technologies. Such directions of future work would not only push the theoretical foundations of the Akbota equation further but also extend its applications in science and engineering.

Acknowledgements

One of the corresponding authors (A.G.) acknowledges the support from the University of Guadalajara, Mexico, through the program PROSNI.

Declarations

Author contributions Conceptualization: B.C., M.Z.B., N.A., M.J., J.E.M.-D. and A.G.; Data curation: B.C., M.Z.B., N.A., M.J., S.M., J.E.M.-D. and A.G.; Formal analysis: B.C., M.Z.B., N.A., M.J., S.M., J.E.M.-D. and A.G.; Funding acquisition: J.E.M.-D. and A.G.; Investigation: B.C., M.Z.B., N.A., M.J., S.M., J.E.M.-D. and A.G.; Methodology: B.C., M.Z.B., N.A., M.J., J.E.M.-D. and A.G.; Project administration: J.E.M.-D. and A.G.; Resources: B.C., M.Z.B., N.A., M.J., S.M., J.E.M.-D. and A.G.; Software: B.C., M.Z.B., N.A., M.J., S.M., J.E.M.-D. and A.G.; Supervision: B.C., M.Z.B., N.A., M.J., J.E.M.-D. and A.G.; Validation: B.C., M.Z.B., N.A., M.J., S.M., J.E.M.-D. and A.G.; Visualization: B.C., M.Z.B., N.A., M.J., S.M., J.E.M.-D. and A.G.; Roles/Writing – original draft: B.C., M.Z.B., N.A., M.J., S.M., J.E.M.-D. and A.G.; Writing – review & editing: B.C., M.Z.B., N.A., M.J., S.M., J.E.M.-D. and A.G.

All authors approved the submitted version of this manuscript.

Conflict of interest declaration The authors declare no potential conflict of interest.

Data availability statement Data sharing not applicable — no new data generated.

References

[1] D. Baldwin and W. Hereman. Symbolic software for the Painlevé test of nonlinear ordinary and partial differential equations. *Journal of Nonlinear Mathematical Physics*, 13(1):90–110, 2006.

[2] A. S. Fokas. Symmetries and integrability. *Studies in Applied Mathematics*, 77(3):253–299, 1987.

[3] A. M. Wazwaz. A new fifth-order nonlinear integrable equation: multiple soliton solutions. *Physica Scripta*, 83(1):015012, 2011.

[4] J. A. Sanders and J. P. Wang. Integrable systems and their recursion operators. *Nonlinear Analysis: Theory, Methods and Applications*, 47(8):5213–5240, 2001.

[5] F. Verheest, C. P. Olivier, and W. A. Hereman. Modified Korteweg–de Vries solitons at supercritical density in two-electron temperature plasmas. *Journal of Plasma Physics*, 82(2):905820208, 2016.

[6] M. S. Osman and J. A. T. Machado. New nonautonomous combined multi-wave solutions for (2+1)-dimensional variable coefficients KdV equation. *Nonlinear Dynamics*, 93(2):733–740, 2018.

[7] C. M. Khalique. Solutions and conservation laws of Benjamin–Bona–Mahony–Peregrine equation with power-law and dual power-law nonlinearities. *Pramana*, 80(3):413–427, 2013.

[8] A. M. Wazwaz. *Partial Differential Equations and Solitary Waves Theory*. Springer Science and Business Media, Berlin, 2010.

[9] R. Hirota. A new form of Bäcklund transformations and its relation to the inverse scattering problem. *Progress of Theoretical Physics*, 52(5):1498–1512, 1974.

[10] D. E. Baldwin and W. A. Hereman. A symbolic algorithm for computing recursion operators of nonlinear partial differential equations. *International Journal of Computer Mathematics*, 87(5):1094–1119, 2010.

[11] H. Leblond and D. Mihalache. Models of few optical cycle solitons beyond the slowly varying envelope approximation. *Physics Reports*, 523(2):61–126, 2013.

[12] H. Leblond and D. Mihalache. Few-optical-cycle solitons: modified Korteweg–de Vries sine-Gordon equation versus other non–slowly-varying-envelope-approximation models. *Physical Review A*, 79(6):063835, 2009.

[13] W. A. Hereman. Symbolic computation of conservation laws of nonlinear partial differential equations in multi-dimensions. *International Journal of Quantum Chemistry*, 106(1):278–299, 2006.

[14] A. M. Wazwaz. A new generalized fifth-order nonlinear integrable equation. *Physica Scripta*, 83(3):035003, 2011.

[15] M. S. Osman and J. A. T. Machado. The dynamical behavior of mixed-type soliton solutions described by (2+1)-dimensional Bogoyavlensky–Konopelchenko equation with variable coefficients. *Journal of Electromagnetic Waves and Applications*, 32(11):1457–1464, 2018.

[16] I. S. Krasil'shchik and P. H. Kersten. *Symmetries and Recursion Operators for Classical and Supersymmetric Differential Equations*, volume 507 of *Mathematics and Its Applications*. Springer Science and Business Media, Dordrecht, 2013.

[17] H. Liu. Generalized symmetry classifications, integrable properties and exact solutions to the general nonlinear diffusion equations. *Communications in Nonlinear Science and Numerical Simulation*, 36:21–28, 2016.

[18] T. Motsepa. *Symmetry analysis, conservation laws and exact solutions of certain nonlinear partial differential equations*. PhD thesis, North-West University (South Africa), Mafikeng Campus, 2016.

[19] P. A. Clarkson and C. M. Cosgrove. Painlevé analysis of the non-linear Schrödinger family of equations. *Journal of Physics A: Mathematical and General*, 20(8):2003–2024, 1987.

[20] M. Lakshmanan and R. Sahadevan. Painlevé analysis, Lie symmetries, and integrability of coupled nonlinear oscillators of polynomial type. *Physics Reports*, 224(1-2):1–93, 1993.

[21] S. S. Ray. Painlevé analysis, group invariant analysis, similarity reduction, exact solutions, and conservation laws of Mikhailov–Novikov–Wang equation. *International Journal of Geometric Methods in Modern Physics*, 18(06):2150094, 2021.

[22] S. Ur-Rehman and J. Ahmad. Dynamics of optical and multiple lump solutions to the fractional coupled nonlinear Schrödinger equation. *Optical and Quantum Electronics*, 54(10):640, 2022.

[23] E. Yomba. The modified extended Fan sub-equation method and its application to the (2+1)-dimensional Broer–Kaup–Kupershmidt equation. *Chaos, Solitons and Fractals*, 27(1):187–196, 2006.

[24] H. Zhang. A note on some sub-equation methods and new types of exact travelling wave solutions for two nonlinear partial differential equations. *Acta Applicandae Mathematicae*, 106(2):241–249, 2009.

[25] M. A. S. Murad, W. A. Faridi, M. Iqbal, A. H. Arnous, N. A. Shah, and J. D. Chung. Analysis of Kudryashov's equation with conformable derivative via the modified Sardar sub-equation algorithm. *Results in Physics*, 60:107678, 2024.

[26] T. Shahzad, M. Z. Baber, M. Qasim, T. A. Sulaiman, M. W. Yasin, and N. Ahmed. Explicit solitary wave profiles and stability analysis of biomembranes and nerves. *Modern Physics Letters B*, page 2450305, 2024.

[27] N. H. Aljahdaly. Some applications of the modified $(\frac{G'}{G^2})$-expansion method in mathematical physics. *Results in Physics*, 13:102272, 2019.

[28] P. G. Estévez. Darboux transformation and solutions for an equation in 2+1 dimensions. *Journal of Mathematical Physics*, 40(3):1406–1419, 1999.

[29] A. Hussain, M. Usman, and F. Zaman. Lie group analysis, solitons, self-adjointness and conservation laws of the nonlinear elastic structural element equation. *Journal of Taibah University for Science*, 18(1):2294554, 2024.

[30] M. J. Ablowitz. Nonlinear waves and the inverse scattering transform. *Optik*, 278:170710, 2023.

[31] M. Z. Baber, G. Abbas, I. Saeed, T. A. Sulaiman, N. Ahmed, H. Ahmad, et al. Optical solitons for 2D-NLSE in multimode fiber with Kerr nonlinearity and its modulation instability. *Modern Physics Letters B*, page 2450341, 2024.

[32] M. Ozisik, A. Secer, and M. Bayram. Obtaining analytical solutions of (2+1)-dimensional nonlinear Zoomeron equation by using modified F-expansion and modified generalized Kudryashov methods. *Engineering Computations*, 41(5):1105–1120, 2024.

[33] S. Tarla, K. K. Ali, and R. Yilmazer. Newly modified unified auxiliary equation method and its applications. *Optik*, 269:169880, 2022.

[34] T. Mathanaranjan and R. Myrzakulov. Integrable Akbota equation: conservation laws, optical soliton solutions and stability analysis. *Optical and Quantum Electronics*, 56(4):564, 2024.

[35] S. T. Rizvi, A. R. Seadawy, and S. Ahmed. Bell and kink type, Weierstrass and Jacobi elliptic, multiwave, kinky breather, M-shaped and periodic-kink-cross rational solutions for Einstein's vacuum field model. *Optical and Quantum Electronics*, 56(3):456, 2024.

[36] Y. L. Ma, A. M. Wazwaz, and B. Q. Li. Soliton resonances, soliton molecules, soliton oscillations and heterotypic solitons for the nonlinear Maccari system. *Nonlinear Dynamics*, 111(19):18331–18344, 2023.

[37] Y. L. Ma and B. Q. Li. Bifurcation solitons and breathers for the nonlocal Boussinesq equations. *Applied Mathematics Letters*, 124:107677, 2022.

[38] M. H. Khan and A. M. Wazwaz. Lump, multi-lump, cross kinky-lump and manifold periodic-soliton solutions for the (2+1)-dimensional Calogero–Bogoyavlenskii–Schiff equation. *Heliyon*, 6(4):e03824, 2020.

[39] S. Ahmed, A. R. Seadawy, S. T. Rizvi, and A. M. Mubaraki. Homoclinic breathers and soliton propagations for the nonlinear (3+1)-dimensional Geng dynamical equation. *Results in Physics*, 52:106822, 2023.

[40] B. Ceesay, M. Z. Baber, N. Ahmed, A. Akgül, A. Cordero, and J. R. Torregrosa. Modelling symmetric ion-acoustic wave structures for the BBMPB equation in fluid ions using Hirota's bilinear technique. *Symmetry*, 15(9):1682, 2023.

[41] M. Wang, B. Tian, Q. X. Qu, X. H. Zhao, Z. Zhang, and H. Y. Tian. Lump, lumpoff, rogue wave, breather wave and periodic lump solutions for a (3+1)-dimensional generalized Kadomtsev–Petviashvili equation in fluid mechanics and plasma physics. *International Journal of Computer Mathematics*, 97(12):2474–2486, 2020.

[42] X. W. Yan, S. F. Tian, M. J. Dong, L. Zhou, and T. T. Zhang. Characteristics of solitary

wave, homoclinic breather wave and rogue wave solutions in a (2+1)-dimensional generalized breaking soliton equation. *Computers and Mathematics with Applications*, 76(1):179–186, 2018.

[43] S. Kumar and B. Mohan. A novel and efficient method for obtaining Hirota's bilinear form for the nonlinear evolution equation in $(n+1)$ dimensions. *Partial Differential Equations in Applied Mathematics*, 5:100274, 2022.

[44] S. A. Alsallami, S. T. Rizvi, and A. R. Seadawy. Study of stochastic–fractional Drinfel'd–Sokolov–Wilson equation for M-shaped rational, homoclinic breather, periodic and kink-cross rational solutions. *Mathematics*, 11(6):1504, 2023.

[45] T. Mathanaranjan and R. Myrzakulov. Integrable Akbota equation: conservation laws, optical soliton solutions and stability analysis. *Optical and Quantum Electronics*, 56(4):564, 2024.

[46] H. Y. Kong and R. Guo. Dynamic behaviors of novel nonlinear wave solutions for the Akbota equation. *Optik*, 282:170863, 2023.

[47] M. S. Khan, R. King, and I. L. Hudson. Transmuted modified Weibull distribution: properties and application. *European Journal of Pure and Applied Mathematics*, 11(2):362–374, 2018.

[48] L. Marsavina, A. D. Nurse, L. Braescu, and E. M. Craciun. Stress singularity of symmetric free-edge joints with elasto-plastic behaviour. *Computational Materials Science*, 52(1):282–286, 2012.

[49] Z. Li and S. Zhao. Bifurcation, chaotic behavior and solitary wave solutions for the Akbota equation. *AIMS Mathematics*, 9(8):22590–22601, 2024.

[50] M. M. Tariq, M. B. Riaz, and M. Aziz ur Rehman. Investigation of space-time dynamics of Akbota equation using Sardar sub-equation and Khater methods: unveiling bifurcation and chaotic structure. *International Journal of Theoretical Physics*, 63(8):213, 2024.

[51] M. Awadalla, A. Taishiyeva, R. Myrzakulov, J. Alahmadi, A. A. Zaagan, and A. Bekir. Exact analytical soliton solutions of the M-fractional Akbota equation. *Scientific Reports*, 14(1):13360, 2024.

[52] W. A. Faridi, M. A. Bakar, M. B. Riaz, Z. Myrzakulova, R. Myrzakulov, and A. M. Mostafa. Exploring the optical soliton solutions of Heisenberg ferromagnet-type of Akbota equation arising in surface geometry by explicit approach. *Optical and Quantum Electronics*, 56(6):1046, 2024.

[53] B. Ceesay, N. Ahmed, and J. E. Macías-Díaz. Construction of M-shaped solitons for a modified regularized long-wave equation via Hirota's bilinear method. *Open Physics*, 22(1):20240057, 2024.

[54] B. Ceesay, N. Ahmed, M. Z. Baber, and A. Akgül. Breather, lump, M-shape and other interaction for the Poisson–Nernst–Planck equation in biological membranes. *Optical and Quantum Electronics*, 56(5):853, 2024.

[55] D. U. Ozsahin, B. Ceesay, M. Z. Baber, N. Ahmed, A. Raza, M. Rafiq, et al. Multiwaves, breathers, lump and other solutions for the Heimburg model in biomembranes and nerves. *Scientific Reports*, 14(1):10180, 2024.